




Research Article



Effect of silica and lignocellulosic additives on the formation and the distribution of meso and macropores in foam metakaolin-based geopolymer filters for dyes and wastewater filtration

Martine Youmoue^{1,2}  · Rufin Théophile Tene Fongang³ · Ameni Gharzouni² · Rodrigue Cyriaque Kaze⁴ · Elie Kamseu³ · Vincenzo M. Sglavo⁵ · Ignas Tonle Kenfack¹ · Benoit Nait-Ali² · Sylvie Rossignol²

Received: 19 November 2019 / Accepted: 2 March 2020 / Published online: 13 March 2020
© Springer Nature Switzerland AG 2020

Abstract

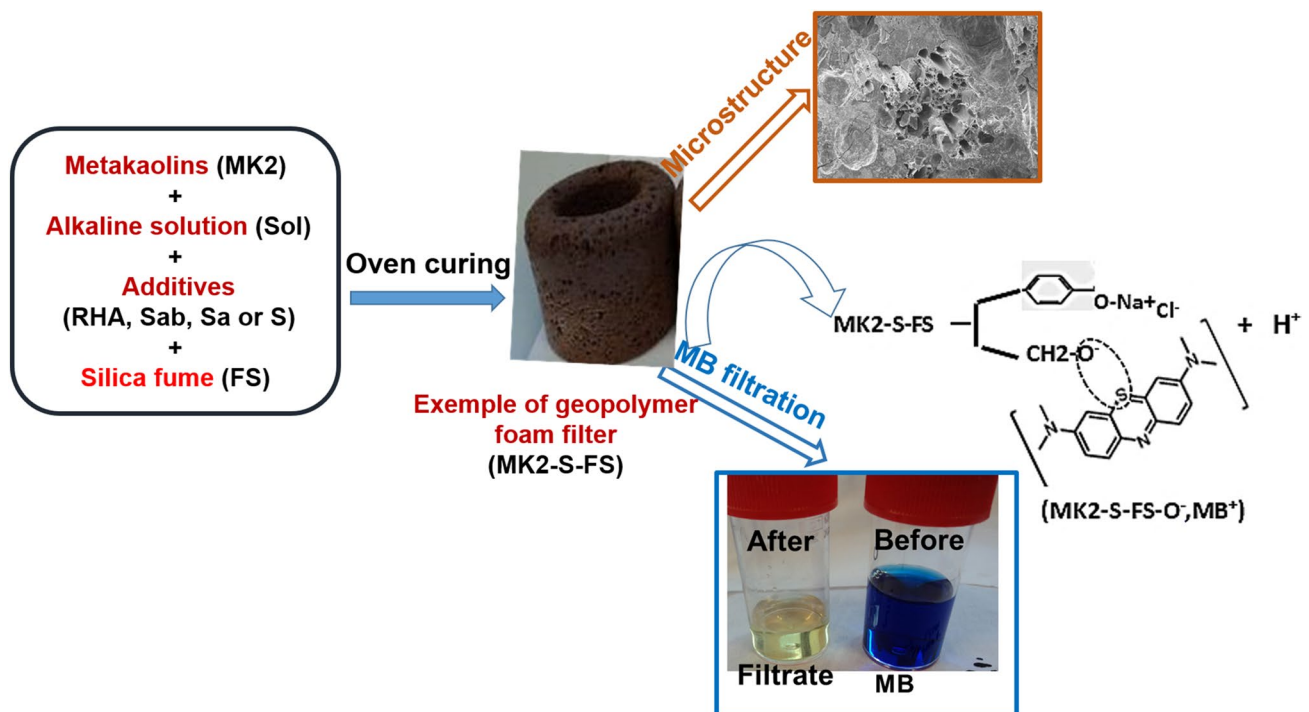
This work investigates how silica and lignocellulose additives affect the production of metakaolin based-geopolymer foam filters. Lignocellulosic material from wood powder sawdust (S), silica from rice husk ash (RHA), calcined (Sa) and uncalcined (Sab) sand were separately used together with high amorphous silica fume (foaming agent) and integrated into the matrix (metakaolin and solution). The different geopolymer pastes were cured at 70 °C to enhance the pore formation. Results presented the geopolymer foams filter as sponge-like composites having 58–68% of porosity with 1–4 MPa of compressive strength. RHA and Sa lead to materials with more meso and macropores. Sawdust based-geopolymer (the hardest foam) containing channel pores predominated by coarse pores exhibited a flow rate of 4 mL min⁻¹. The absence of the bands of MB from FT-IR spectra and UV spectra (663 nm) of MB filtrate (totally blue discoloured) indicated that, geopolymers foams filters designed are suitable for dyes and wastewater filtration.

✉ Martine Youmoue, youmstina@yahoo.fr; martine.youmoue@univ-dschang.org; ✉ Sylvie Rossignol, sylvie.rossignol@unilim.fr | ¹RU-NOCHEE, Research Unit of Noxious Chemistry and Environmental Engineering, Faculty of Science, University of Dschang, P.O. Box 67, Dschang, Cameroon. ²UMR CNRS 7315, CEC, Institut de Recherche sur les céramiques (IRCER), Université de Limoges, 12 Rue Atlantis, Limoges, France. ³Local Materials Promotion Authority (MIPROMALO), P.O. Box 2396, Yaounde, Cameroon. ⁴Laboratory of Applied Inorganic Chemistry, Faculty of Science, University of Yaoundé I, P.O. Box 812, Yaoundé, Cameroon. ⁵Department of Materials Engineering and Industrial Technologies, University of Trento, Via Mesiano 77, 38050 Trento, Italy.



SN Applied Sciences (2020) 2:642 | <https://doi.org/10.1007/s42452-020-2388-x>

Graphic abstract



Keywords Meso and macro pores · Silica · Lignocellulosic · Geopolymers · Foams · Filters

1 Introduction

Geopolymers are known as three-dimensional network inorganic materials obtained through polycondensation process when aluminosilicates source materials are mixed with silicate and alkaline solutions [1, 2]. They exhibit wide properties such as excellent bond strength, high compressive strength, low shrinkage, good fired resistance, good durability and acid resistance [3, 4]. These past decades, the ability of geopolymer materials to adsorb and immobilize toxic metals [5–7] have been carried out. The separation process through the use of geopolymer membranes is also being increased with interest although most of the works have been focused on low pores range materials [8–11]. However, as observed by Lin and Lan [12], there are some properties that cannot be achieved by conventional dense materials; therefore the need of designing porous materials membrane for filtration. The ease of controlling the porosity of geopolymers confers to them numerous pore network behavior. However, the used of agent foaming like nano aluminum powders remain expensive and toxic, thus limiting their use. Therefore, the use of silica source as porous agent from biomass appears as low cost and environmentally friendly.

Various methods of producing porous geopolymers have been reported by many researchers. The usage of by-products (rice husk ashes, sawdust, cotton stalk fiber) to improve pore-related properties such as density, microstructure, and thermal conductivity is well established [13, 15–20]. For example, Tene et al. [13] and Ngouloure et al. [14] demonstrated that lightweight metakaolin-based geopolymers reinforced by sawdust and rice husk ash exhibited good properties for thermal insulation application, respectively. Rasouli et al. [21] introduced polylactic acid fibers with different diameters to fabricate well-aligned microporous metakaolin based geopolymer by extrusion method. Their results revealed that porous bodies synthesized with smallest polylactic acid fibers diameter exhibit higher water permeability.

In addition, another classes of pore-forming agent commonly used in geopolymer technology is silica fume [22–25]. Silica fume is a micro silica by-product derives from the production of silicon and ferrosilicon alloys through the reduction of high pure quartz with coal in electric furnace [23]. This technique offers the advantage to allow sponge-like structure through dihydrogen generation in alkaline medium from the reaction between free silicon (in silica fume powder) with alkaline solution [22].

This synthesis condition favored the production of bubbles of hydrogen (H_2) gas within the geopolymer system and consequently the volume expansion of the geopolymer as reported by Luna-Galiono et al. [25]. The efficiency of silica-based materials to attach bacteria or virus to their surfaces in one hand and the durability of geopolymers reinforced by quartz sand [26] in another hand motivated their choice in this work.

A common supplementary procedure use to increase the porosity of geopolymer is to submit the matrix to a low curing temperature or simultaneously by adding the foaming agent and then cured [27–31]. Siyal et al. [32] described how the curing of geopolymer at low temperature (40 °C) led to a slow geopolymerization reaction with low setting time. In contrast, increase oven curing between 60 and 80 °C accelerates the setting time and the geopolymerization reaction. The investigation of Nasvi et al. [33] focused rather on the effect of temperature on the permeability of geopolymers showed that the range of temperature to design geopolymer allowing the permeation of CO_2 gas was between 23 and 70 °C. This resulting in coarse pore formation and increase of permeability related to weak microstructure. Permeability is defined as a property of materials that lets fluids to diffuse through it to another medium without chemically or physically affecting it. As mentioned a half century ago by Childs [34] one can relate the water permeability of a porous material to the geometry of the boundary between the solid component and the pore space. The possibility of using silica and biomass products to monitor the pore network and filtering properties of geopolymer foams candle filters could then be evaluated.

The removal of dye from water was conducted this decade because of pollution linked to the excess use of dye from dyeing, paper and textile industries etc. [35–37]. Azo dyes are known as carcinogenic and their concentration in drinking water was fixed at $3.1 \mu g L^{-1}$ as limit [38]. It causes eutrophication of aquatic life, some harms in human as vomiting and jaundice [37]. It is therefore emergent to remove dye from water. The removal of dye in water is usually performed by adsorption method but this method is limited because it cannot operate continuously [39]. Hence, the choice of filtration that can be achieved in a continuous system. The difficulty to use dense membranes for water clarification or dyes removal which generally proceeds through reverse osmosis and nanofiltration remains to its high energy operating requirement [40]. Few studies carried out on the use of porous geopolymer as membrane filtration. As example, Bai and Colombo [41] successfully used peroxygen (H_2O_2) and white egg as surfactant to produce porous geopolymer membrane as potential materials for membrane application. Taking into account the toxicity of azo-dye mentioned above, and the

lack of works on highly porous geopolymer membranes. It is interesting to propose porous system from metakaolin and waste biomass for waste water treatment.

The main objective of this work is to study the feasibility to design geopolymer foam filters using metakaolin, silica sources, lignocellulosic material and silica fume. The paper describes the effect of silica sources from rice husk ashes (RHA), semi crystalline silica from calcinated sand (Sa), crystalline silica from raw sand (Sab), and lignocellulosic material from sawdust (S) on the formation and the distribution of meso and macropores in metakaolin based geopolymers filters. Silica fume (FS) foam agent were incorporated together with each of the previous additives into metakaolin powder in alkaline media, and then oven cured for pore formation and volume expansion. Cylindrical specimens and candle geopolymer foam filters were elaborated and characterized. The filtering properties of filter samples were evaluated through the filtration of a methylene blue solution and the characterization of solutions. The resulting geopolymer foam products were also studied using FT-IR spectroscopy, X-ray diffraction (XRD), optical microscope, Scanning Electron Microscope (SEM), simultaneous thermal analysis (TGA and DTA). The performance characteristic was evaluated by means of compressive strength. The permeability was evaluated through the water flowing test. The filtration of MB dye and the characterization of the filtrate using UV-Vis spectrophotometry were also performed.

2 Experimental procedure

2.1 Starting materials

2.1.1 Raw powder materials

Reddish-colored metakaolin (MK2) 100 μm mesh, semi-crystalline calcined sand 700 °C (Sa) ($\leq 400 \mu m$) and Ayous (*Triplochiton scleroxylon*) sawdust ($\leq 400 \mu m$) labeled S collected in a wood factory in Yaounde (Cameroon) all described in the previous work [42] were used as precursors. Metakaolin MK2 was obtained by calcining (collected from Mayoum West Cameroon) kaolinite clay at 700 °C at $5 \text{ }^\circ\text{C min}^{-1}$ of heating rate with 4 h of holding time in Insuni-Mic model electrical furnace. It contains 51.15 wt%, 30.01 wt% and 2.63 wt% respectively of Al_2O_3 , SiO_2 and Fe_2O_3 as main oxides. Raw sand labeled (Sab) supplied by MIPROMALO and RHA were also used as additives. Calcined an uncalcined sand consist of $\sim 98\%$ SiO_2 . Rice husk ah (RHA) used in this work was collected from Ndup (North-West region of Cameroon) and calcined up to 800 °C in an uncontrolled atmosphere in rice production area. The chemical compositions of RHA showed 93.16 of

SiO₂ and 3.11 wt% of K₂O and 0.22 wt% as main oxides. Quartz was found as main mineral phase, with hematite as secondary mineral phase in MK2, Sab and Sa while cristobalite and tridymite predominated RHA. Lignocellulosic sawdust has evidently amorphous α-cellulose at XRD. Silica fume powder (FS), used as pore-forming agent containing around 97.2 wt% SiO₂, 0.7 wt% of free silicon, 0.275 wt% of free carbon was supplied by Ferropem-France.

2.1.2 Chemical reagents and alkaline solution

Commercial sodium silicate solution provided from Woeller Laboratory in Germany and contains 27.5, 8.50 and 64.2 wt% of SiO₂, Na₂O and H₂O respectively. Sodium hydroxide pellets of 97% purity were supplied by Carlo Erba Reagent, France. The alkaline solution used as hardener was prepared as follows. Firstly, NaOH pellets and sodium silicate were weighed on appropriate weight ratios

and mechanically stirred at 850 rpm for 5 min before adding powder. The Si/Na molar ratio of alkaline solution (Sol) was 0.71.

2.2 Procedure of synthesis of porous geopolymers: specimens and candle filters

Geopolymer formulations were elaborated with each of these additives (RHA, Sab, Sa and S) together with silica fume (FS) by mixing them with metakaolin MK2 in the presence of alkaline solution (Si/Na molar ration of 0.71). The mixture was stirred for about 5 min until a homogeneous paste was obtained; The paste was poured into sealed cylindrical polyethylene mold for cylindrical specimens (28 mm diameter and 12 mm of height) and into an appropriate mold (sealed) for candle (pot) shape filters, then kept in oven at 70 °C; Then removed from oven demolded and stored in plastic bags. Geopolymer compositions

Table 1 Nomenclature and compositions of geopolymer foams [(MK₂_{1-x})X_xFS_y]; 1 - x: wt% of metakaolin MK2; x: wt% of X additives partially substituted into metakaolin MK2; y: wt% of FS foaming agent

Formulations	Additives	Foaming agent	wt% in the powder			wt% in the mixture			Synthesis conditions
			MK2	X	FS	Geo (MK2+Sol)	X	FS	
	X	FS	1-x	x	y				
(a) MK2-0 (Ref)	/	/	100	0	0	100	0	0	20 °C/24 h
(b) MK2-FS	/	FS	71	0	29	87	0	13	70 °C/(< 24 h)
(c) MK2-RHA-FS	RHA		62.5	12.5	25	82	6	12	
(d) MK2-Sab-FS	Sab								
(e) MK2-Sa-FS	Sa								
(f) MK2-S-FS	S								

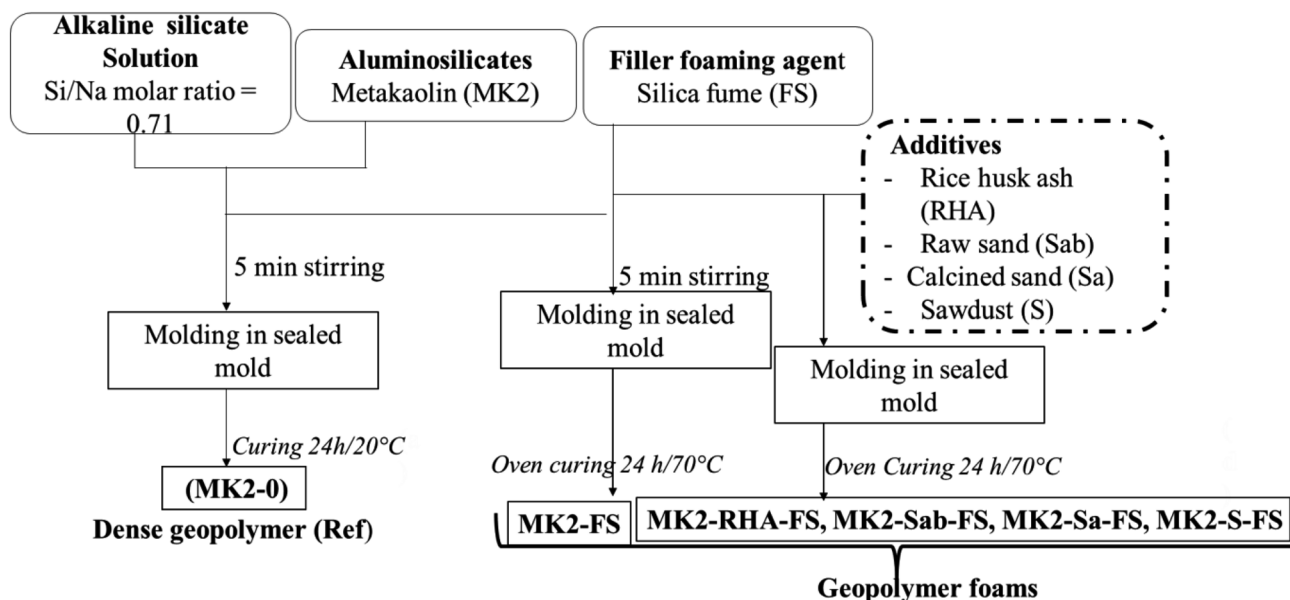


Fig. 1 Synthesis protocol of dense geopolymer and foam geopolymer filters

Table 2 Theoretical Si/Al, Si/Na and Na/Al molar ratios; pH value of water, bulk and relative densities, porosity Φ of geopolymer samples

Compositions	Si/Al	Si/Na	Na/Al	pH (± 0.1)	Bulk density ρ (g cm ⁻³)	Porosity Φ (%)	Compressive strength σ (MPa)
(a) MK2-0	2.42	1.77	1.37	12.0	1.78 \pm 0.02	15 \pm 0.48	66 \pm 1
(b) MK2-FS	3.72	2.27	1.64	11.4	0.65 \pm 0.04	68 \pm 0.81	1 \pm 0.2
(c) MK2-RHA-FS	4.25	2.59		11.0	0.90 \pm 0.02	59 \pm 0.89	3 \pm 0.5
(d) MK2-Sab-FS	4.28	2.61		10.8	1.01 \pm 0.06	59 \pm 1.30	3 \pm 0.5
(e) MK2-Sa-FS	4.28	2.61		10.7	0.88 \pm 0.10	58 \pm 1.16	3 \pm 0.4
(f) MK2-S-FS	3.72	2.27		12.0	0.81 \pm 0.01	61 \pm 0.85	4 \pm 0.2

formula were given as follows: [(MK2_b Sol_a)] used as the reference sample; [(MK2_{1-x} FS_y)_b Sol_a] for foam without additives and [(MK2_{1-x}) X_x FS_y]_b Sol_a] for foam composites containing additives where,

- «1 - x» is the wt% of metakaolin MK2
- «x» the wt% of X additive (RHA, Sab, Sa and S)
- «y» the wt% of FS
- «a» the wt% of alkaline solution (Sol)
- and «b» the wt% of overall powder (MK2 + X+FS)

[(MK2_{0.41} Sol_{0.59})], [(MK2_{0.625} RHA_{0.125} FS_{0.25})_{0.48} Sol_{0.52}], [(MK2_{0.625} Sab_{0.125} FS_{0.25})_{0.48} Sol_{0.52}], [(MK2_{0.625} Sa_{0.125} FS_{0.25})_{0.48} Sol_{0.52}], [(MK2_{0.625} S_{0.125} FS_{0.25})_{0.48} Sol_{0.52}] samples were labelled MK2-0, MK2-RHA-FS, MK2-Sab-FS, MK2-Sa-FS and MK2-S-FS, respectively. The compositions of elaborated geopolymer samples are presented on Table 1, the synthetic protocol on Fig. 1 and their photos on Fig. 6. The theoretical Si/Al, Si/Na and Na/Al molar ratios of geopolymer samples are given on Table 2.

2.3 Characterization methods

Many physico-chemical techniques were used to characterize the resulting geopolymer products namely MK2-0, MK2-FS, MK2-RHA-FS, MK2-Sab-FS, MK2-Sa-FS and MK2-S-FS and the filtrate solutions.

X-ray powder diffraction of samples was carried out on a Bruker AXS D8 Advance diffractometer (λ Cu-K α =1.541 Å between 3 and 75 2 θ range applying a pitch of 0.015 s and a speed of 0.5°/min. The apparatus was controlled by Winzar software, phase identification was performed with the EVA software by comparing the pdf of minerals phases obtained with the pdf ICC data.

Structural analysis of powder samples was determined on FT-IR Bruker spectrometer using OMNIC Nicolet software. The spectra were recorded between 4000 and 400 cm⁻¹ with a resolution of 4 cm⁻¹.

Thermogravimetric analysis (TG) coupled with Differential Thermal Analysis (DT) were performed on STD

Q600 apparatus TA Instrument piloted by Thermal Analysis 2000 software. Using platinum crucibles. The analysis was performed between 30 and 800 °C at the rate of 5 °C min⁻¹ (isotherm of 15 min at 800 °C) under dry air flow (100 mL min⁻¹).

The macrostructures of geopolymers foams were observed with 101T-M7, 7", 2MP micro camera Ceramic instrument Model optical microscope.

Microstructure and morphology of the geopolymers samples were observed on a Quanta 450 DELEF FEI Scanning Electron Microscope (SEM) at 10 kv coupled with an Energy Dispersive Spectrometry (EDS) apparatus. Samples were firstly coated with silver solution. The images observed in secondary electron (SE) mode were registered at several magnifications.

Mercury intrusion porosimetry (MIP) technique is used to bring out data on pore size(s), average pore size and pore-size distribution in materials. But nanopores and air bubbles pores are not taking in account during the MIP analysis. An Autopore 2000 porosimeter working from 0.1 to 50,000,000 psia with pore size radius from 0.03 to 490 μ m was used to obtain the pore size distribution, the relative and specific intruded volume in porous geopolymers samples.

Relative density (ρ) of geopolymer samples were determined using Helium Micrometrics AccuPyc 1330 pycnometer; while the bulk density (ρ_a) was obtained from the ratio of the mass over the volume of cylindrical specimens. The porosity Φ (%) of samples was calculated from Eq. 5 (Eq. 1) [43]. Results are a mean of three samples for each formulation. The values of the porosity of geopolymer samples are given in Table 1.

$$\Phi(\%) = \left(1 - \frac{\rho_a}{\rho}\right) * 100 \quad (1)$$

The compressive strengths of samples aged for 7 days (cylindrical specimen with of ~45 mm height and 28 mm diameter) were tested. An Instron instrument using 50 KN pre-charged operating at a crosshead speed of 0.5 mm s⁻¹ were used to obtained the strength F (N). The compressive

strength (σ , MPa) was obtained according to Eq. 1 (Eq. 2). The values of masses and dimensions of a cylindrical geopolymer pieces were measured before the compressive test in order to calculate the bulk density (ρ_b) (see Eq. 1) and the surface (S) of specimens. Results give here (porosity and compressive strengths) are the averages of three values obtained from each geopolymer composition. The photos of cylindrical geopolymer foams rectified before compressive test are given in Fig. 6A.

$$\sigma = \frac{F}{S} \tag{2}$$

where F is the strength (in N) and S the surface (in m^2) of cylindrical sample.

Geopolymer samples were soaked in deionized water for 24 h. A WTW 3310 pH-meter (25 °C) equipped with electrodes was used to record the pH values of water from each specimen as well as the pH value of the filtrate.

Permeability test was performed by simply collecting the volume of flow liquid (deionized water) through geopolymer candle filters over time. And then, the plot of the cumulated volume in function of flowing time was plotted. Filtration feasibility was carried out as follow: A volume of waste solution (methylene blue solution) was poured into the filter and the liquid flowed through the filter was collected. Any pressure was applied, so the filtration was performed at atmospheric pressure. The photos of methylene blue filtration are presented in Fig. 2.

Varian UV–Vis spectrophotometer working with Scan-Offline software was used to analyse the methylene blue solution and its filtrate at the interval (300 and 750 nm) of wavelength (λ) and a scan rate of 4 nm s^{-1} . MB solutions with different concentration was also prepared to plot the calibration line (Fig. 10B), used to obtained the concentration of the filtrate solutions (C) from Beer Lambert equation (Eq. 3).

$$A = \epsilon lc \tag{3}$$

where ϵ is the molar extinction coefficient of solution ($L \text{ g}^{-1} \text{ cm}^{-1}$ or $L \text{ mol}^{-1} \text{ cm}^{-1}$), l is the length of a polystyrene cell used (10 mm or 1 cm), C the concentration of analysed solution (g L^{-1} or mol L^{-1}) [35]. Then, Eq. 4 was apply to calculate the removal percentage efficiency (R).

$$R = \left(\frac{C_0 - C}{C_0} \right) \times 100 \tag{4}$$

where, C_0 is the initial concentration, C the concentration of the filtrate.

Another Bruker FT-IR spectrometer was used to collect the FTIR spectra of solutions between 4000 and 400 cm^{-1} at a scan rate of $4 \text{ cm}^{-1} \text{ s}^{-1}$ and a resolution of 4 cm^{-1} . The spectra were corrected with a straight line between 2400 and 2280 cm^{-1} therefore to remove the contribution of CO_2 .

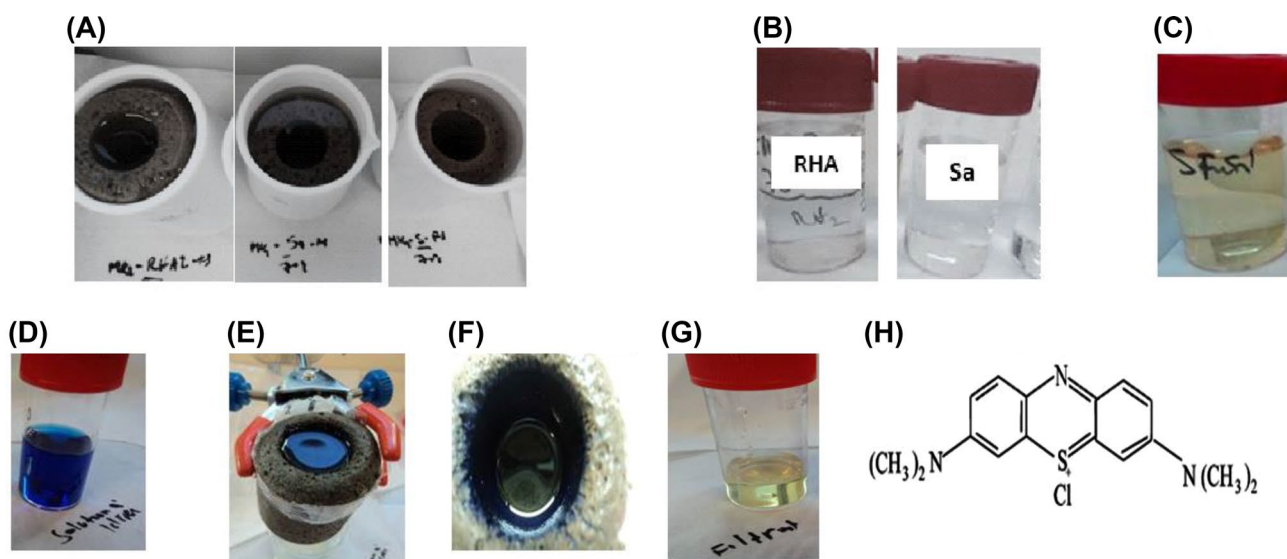


Fig. 2 Soaking of foam filters in deionized water before water flowing test (a); uncoloured water from filters containing silica additives (b) and slightly yellowed coloured water from sawdust based filter (c); Filtration of initial solution of MB of 0.03 g L^{-1} (d), through MK2-

S-FS filter in atmospheric pressure (e), Discolouration of MB solution inside the filter after 2 days (f); Filtrate totally blue discoloured and slightly yellow coloured (g); chemical structure of methylene blue (h)

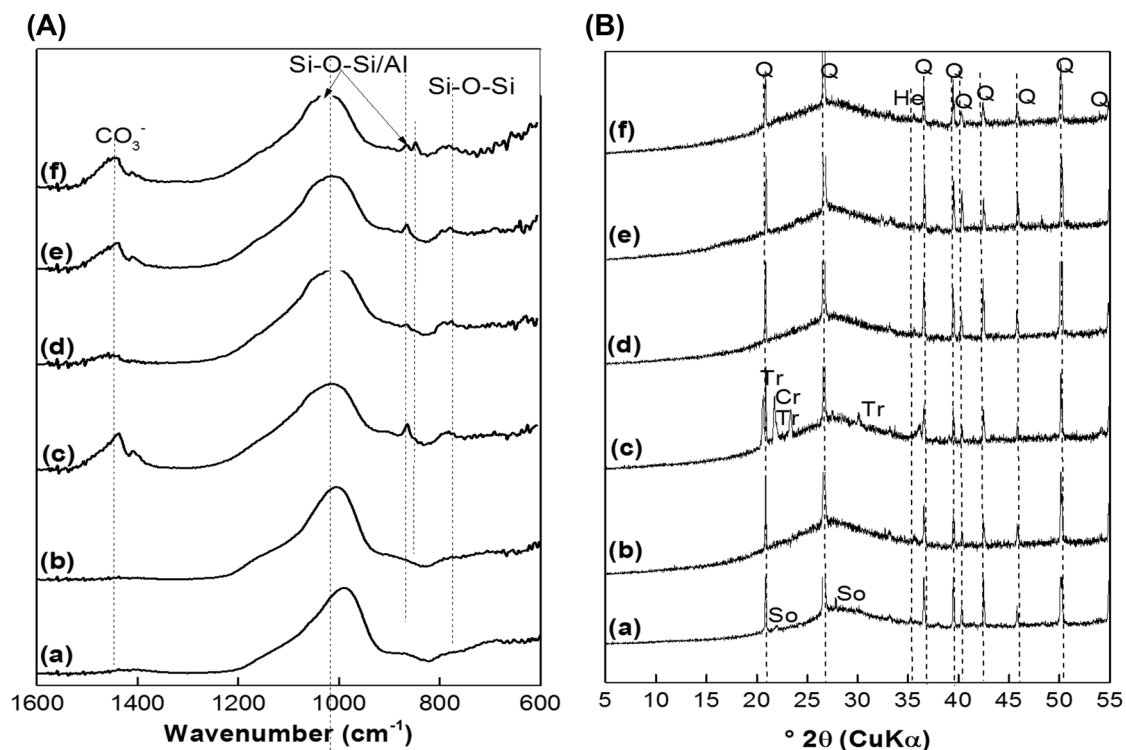


Fig. 3 FT-IR spectra **(A)** and XRD patterns **(B)** of MK2-0 (a), MK2-FS (b), MK2-RHA-FS (c), MK2-Sab-FS (d), MK2-Sa-FS (e) and MK2-S-FS (f) geopolymer samples. Q: Quartz (00-046-1045); Tr: Tridymite (03-0227); Cr: Cristobalite; Hematite (33-664); So: Sodion (04-016-4448)

3 Results and discussion

3.1 Effect of additives on common properties of geopolymer foams

3.1.1 Phase evolution

3.1.1.1 Mineral phases The mineralogy of raw materials used was discussed in our previous work [42]. It was observed on the FT-IR spectra of MK2-0, MK2-FS, MK2-RHA-FS, MK2-Sab-FS, MK2-Sa-FS and MK2-S-FS geopolymer samples (Fig. 3A) that the asymmetric stretching vibration of Si–O–M (M = Si, Al, or Na) is found at 988 cm^{-1} on the spectrum of dense geopolymer (Fig. 3Aa). This band shifted to high value number ($\sim 1024\text{ cm}^{-1}$) on the spectra of foams geopolymer (Fig. 3Ab–f), closed to the findings of Prud'Homme et al. [29] on foam geopolymer, and similar to the results of Zhang et al. [44] and Autef et al. [45] and on dense materials. This is due to the amorphous silica fume used, highly reactive which favoured the Si–O band in the geopolymer network. The Si–O bands located at about $690\text{--}790\text{ cm}^{-1}$ belongs to the quartz mineral from precursors (MK2, Sab and Sa). The carbonate bands occurred at about $1444\text{--}1446\text{ cm}^{-1}$ is formed between the excess of sodium ions from activator solution and CO_2 of the atmospheric air. These bands are more pronounced

in the spectra of geopolymer with additives (RHA, Sab, Sa and S), attributed to their probably low reactivity compared to that of MK2-0 and MK2-FS containing more reactive species. The FT-IR spectrum of MK2-S-FS sample did not show the stretching band of organic compounds (as $-\text{CH}_2-$, $-\text{O}-\text{CH}_2-$ from sawdust). This could be due to the deacetylation of sawdust in alkali media [46–48] resulting in formation organic salts [47, 49]. For example, Of et al. [50] suggested cellulosate is an intermediate compound formed from cellulose in alkali medium through carboxymethyl process at low temperature at $70\text{ }^\circ\text{C}$. In the given work the oven curing at $70\text{ }^\circ\text{C}$, the appearance of the band near 895 cm^{-1} (Fig. 3Af) could be likely attributed to the absorption band of lignocellulosic salts. This band was not found in the spectra of geopolymer foams with silica additives (Fig. 3A1b–f). However, the high intensity of silica band can be made under estimate or erased the weak bands of organic salts expected. This could explain the absence of stretching band of organic compounds in MK2-S-FS sample.

The XRD patterns (Fig. 3B) of geopolymer samples exhibited amorphous phase with a hump at the interval of 20 and $35\text{ }2\theta$ related to geopolymer network footprint. Near to the amorphous structure in geopolymer products, it is noticed the presence of some reflection peaks of crystalline phases such as quartz and hematite. These

phases existing in solid precursors were still present after alkaline activation showing that they seem to be unaltered in alkaline media. However, the quartz's peaks of MK2-Sab-FS sample were more intense compared to that of MK2-Sa-FS. This may suggest the loss of crystallinity of quartz mineral after calcination (700 °C) [51]. The tridymite and cristobalite phases observed on the XRD pattern of MK2-RHA-FS sample (Fig. 3Bc) provided from amorphous RHA (obtained at (800 °C) were also reported by Maulana et al. [52]. In fact, Kaur et al. [53], and Detpman et al. [54] investigated the production of geopolymer with rice hush ash and concluded that the calcination temperature affects the mineralogical phases. It is also important to notice a weak peak of hematite on the XRD pattern of geopolymer samples (Fig. 3Ba–f) related to the precursors used in accordance with literature [55]. Finally, the peak of sodian mineral phase $K_{0.5}Na_{0.5}AlSi_3O_8$ (04-016-4448) occurring on the XRD patterns of geopolymers suggested the probably dissolution of orthose $KAlSi_3O_8$ feldspathic phase from MK2 in alkali medium [29, 56].

3.1.1.2 Thermal behaviour The effect of thermal treatment on the phase evolution was evaluated through the curves of TG/DSC. The TG/DSC curves of MK2-0, MK2-RHA-FS, MK2-Sab-FS, MK2-Sa-FS and MK2-S-FS geopolymer samples are plotted in Fig. 4a–f, respectively. Figure 4a–f revealed the presence of two endothermic peaks at ~70 °C (or at $T < 200$ °C) and at 575 °C in all resultant products. The first corresponds to the dehydration

of physically bonded water and the loss of free water [57–59]. The second peak about ~575 °C is attributed to the polymorphic transformation of α -quartz to β -quartz [60]. This confirms the presence of quartz phase identified in the XRD pattern of all geopolymers foam (Fig. 3B). In addition, several endothermic peaks were observed on the curve of the MK2-S-FS sample at about 300, 400 and 525 °C. These peaks could be directly linked to the decomposition of organic matter (sawdust) which seem to be totally destroyed at 800 °C. According to Ulloa [61], hemicellulose and cellulose decompose at about 350 °C and 500 °C while the destruction of lignin occurs up to 500 °C. So common gas from carbonates species decomposition were supposed to be released. The endothermic peaks between 300 and 500 °C are related to the release of CO_2 , CO , CH_4 , H_2 gases [62, 63] explained by the absorption band appearing at $\sim 895\text{ cm}^{-1}$ on the FT-IR spectrum of MK2-S-FS (Fig. 3Af). The carbonates species could also provide from the excess of Na^+ ions [45] and justify the release of CO during the thermogravimetric analysis.

The weight loss (WL) values of 19, 20, 17, 19, 18, and 26% obtained respectively from MK2-0, MK2-FS, MK2-RHA-FS, MK2-Sab-FS, MK2-Sa-FS and MK2-S-FS geopolymer samples (Fig. 4a–f) were confronted to their theoretical values calculated from the percentage of geopolymer compositions (Table 1) and reference value without additive. The reference (pure geopolymer) without additive corresponding to 100% of "geo" (metakaolin and reactive solution) exhibited 19% of WL (Fig. 4a). MK2-FS sample

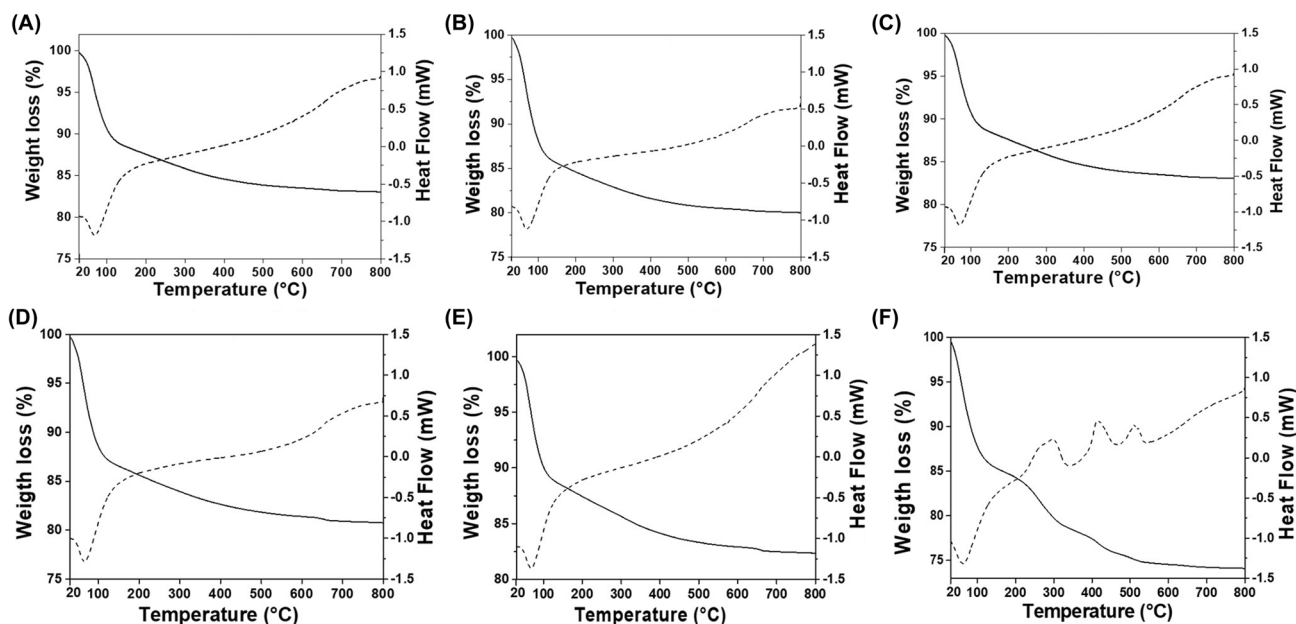


Fig. 4 TG (■) and DTA (—) curves of MK2-0 (a), MK2-FS (b), MK2-RHA-FS (c), MK2-Sab-FS (d), MK2-Sa-FS (e) and MK2-S-FS (f) geopolymer samples

Table 3 Comparison between the theoretical weight loss WL_{the} (calculated using the compositions of the samples from Table 1 and the WL of the reference) and the effective weight loss obtained from TG analysis (WL_{TG}) of geopolymer samples

Geopolymer samples	WL_{the}	WL_{TG}
MK2-0	$(100 \times 19)/100 = 19$	19
MK2-FS	$(87 \times 19)/100 = 17$	20
MK2-RHA-FS	$(82 \times 19)/100 = 16$	17
MK2-Sab-FS	$(82 \times 19)/100 = 16$	19
MK2-Sa-FS	$(82 \times 19)/100 = 16$	18
MK2-S-FS	$(82 \times 19)/100 = 16$	26

containing 87% of “geo” and 13% of FS could theoretically undergo 17% of WL from “geo” and 3% of WL from FS which corroborates with 20% of total WL at 800 °C obtained from TG (Fig. 4b). The four remaining samples (MK2-RHA-FS, MK2-Sab-FS, MK2-Sa-FS and MK2-S-FS) are composed of 82% of “geo”, 6% of additives (RHA, or Sab, or Sa or S) and 12% of FS. The theoretical WL values from “geo” are supposed to be ~ 16%. So, the supplementary value (Table 3) will be provided from the loss of additives (RHA, Sab, Sa, and S) and silica fume (FS). It is observed that the total WL value of MK2-0, MK2-FS, MK2-RHA-FS, MK2-Sab-FS and MK2-Sa-FS geopolymers are more closed and ranged from 17 to 20% (Fig. 4a–e), contrary to MK2-S-FS geopolymer foam sample which exhibited high WL of 26% (Fig. 4f). The trend of the theoretical values is clearly in line with the thermogravimetric analysis. The high weight loss (WL) of sawdust-based geopolymer foams is linked to the total decomposition of volatile compounds in sawdust [62]. While silica crystalline phase transformation in silica additives (RHA, Sab and Sa) concerns elsewhere the transformation of quartz- α to quartz- β up to 570 °C which did not enough affect the weight loss.

3.1.2 Mechanical and physical properties

3.1.2.1 Compressive strength The mechanical behaviour of MK2-0, MK2-FS, MK2-RHA-FS, MK2-Sab-FS, MK2-Sa-FS and MK2-S-FS geopolymer samples were investigated. The curves of the compressive strength as a function of the displacement of MK2-S-FS foam sample (Fig. 5) exhibited plastic failure, confirming that porous geopolymers were effectively designed. From Table 2, it can be shown that the compressive strength of the reference sample MK2-0 cured at 20 °C only for 24h was 66 MPa. Similar trend was reported by the finding of, by Istuque et al. [64] based on metakaolin based geopolymer synthesis incorporating sewage sludge ash. This compressive strength dramatically decreased from 66 MPa for the reference to ~ 1 MPa for MK2-FS specimen. Although the mechanical strengths of geopolymer foams were low, it was found that the addi-

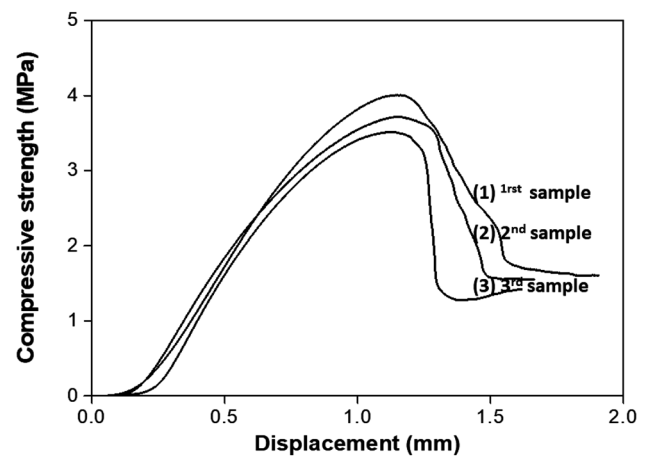


Fig. 5 Compressive strength of MK2-S-FS geopolymer foam undergoing elastic fracture

tion of RHA, Sab, and Sa slightly increased their compressive strength from 1 MPa for MK2-FS to ~ 3 MPa and the addition of sawdust increased up to 4 MPa. The hardest geopolymer foam material was MK2-S-FS sample containing sawdust which acted as mechanical reinforcement, in accordance with the work of Duan et al. [65]. This result can be explained by the fact that lignocellulosic wood fibres acted as bridge within the microstructure of material and therefore improved the mechanical properties. The cellulose (mainly cellulose nanofibers) contained in lignocellulosic materials is recognized as having excellent mechanical properties due to their high crystallinity and length/width aspect ratio, barrier properties, hydrophilicity [66, 67]. Silica fume in the current work did not contribute in improvement of mechanical property in this work as some foam agents described by Bai et al. [68]. But it was interesting to find that the simultaneous combination of filler silica fume FS with other additives allowed the slightly increase of the mechanical properties of geopolymer foams. Moreover, the fast setting of geopolymer paste during the foams formation under oven curing (70 °C) [24, 28] is also responsible of the cracks formation leading to low strength.

3.1.2.2 Density and porosity Table 2 shows that the bulk density value (1.74 g cm^{-3}) of the reference sample was higher compared to that of geopolymer foams ($0.65\text{--}0.90 \text{ g cm}^{-3}$). MK2-FS sample containing only silica fume as additive gave the lowest bulk density (0.65 g cm^{-3}), meaning that the formation of voids was more pronounced, explaining its weak mechanical properties as reported in Sect. 3.1.3. Comparing the additives to each other (RHA, Sab, Sa and S). It was emerged that the addition of lignocellulosic material decreases the density of geopolymer than sand quartz and RHA. This trend was also observed

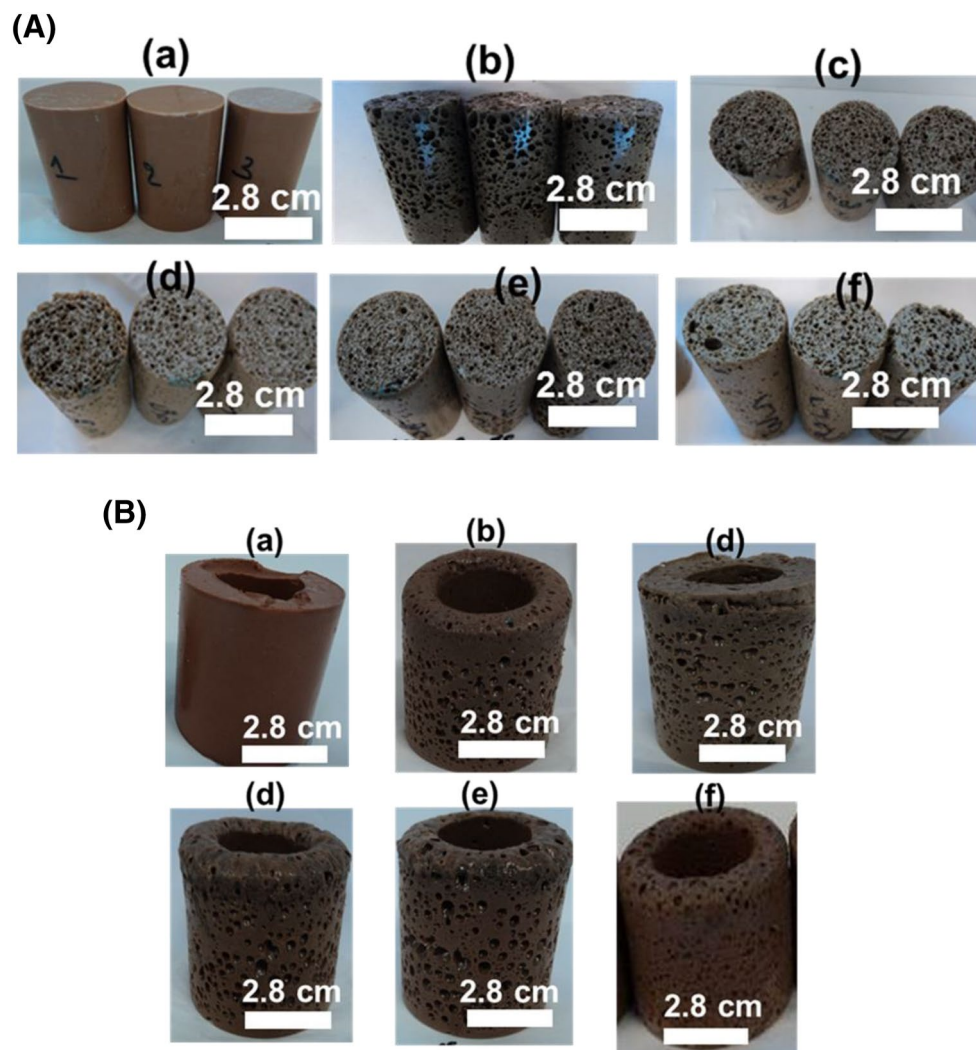


Fig. 6 Photos of the geopolymers' compositions in **A** cylindrical and **B** candle shapes. MK2-0 (a), MK2-FS (b), MK2-RHA2-FS (c), MK2-Sab-FS (d), MK2-Sa-FS (e) and MK2-S-FS (f)

on dense geopolymers obtained with the same precursors in the previous work [42].

The total porosity values (given in Table 2) revealed that the porosity increased from 14 to 68% with the addition of silica fume (foaming agent). A supplementary additional additive of silica (RHA, Sab, Sa) in the previous mixture (metakaolin + alkaline solution + silica fume) highly decreased the porosity (58–59%) than the addition of lignocellulosic material (S) (61%). This trend is in agreement with the bulk density result. These results could be explained by the fact that, there were unreacted phases in RHA, Sab, Sa and S, which did not dissolve in alkaline solution. Then would be likely filled the coarse pores, hence contributed to the reduction of porosity by maintaining the porous structure.

3.1.2.3 pH and adsorption capacity of samples The pH values of water obtained from the immersed geopolymer samples in deionized water for 24 h were recorded (Table 2). It is evidenced that the addition of silica fume accompanied with oven curing (70 °C) to slightly reduced the pH of the medium from 12.05 (for the MK2-0 reference sample) to 10.43–11.33 for geopolymer foams. This could be due to the introduction of silica fume which increases the formation of polysialates and allowed the formation of silanol group [22]. This, resulted in reduction of the degree of basicity, by influencing the equilibrium involved and consequently modified the pH. The elaborated geopolymer filters seem to be good candidates for highly acidic industrial waste water filtration.

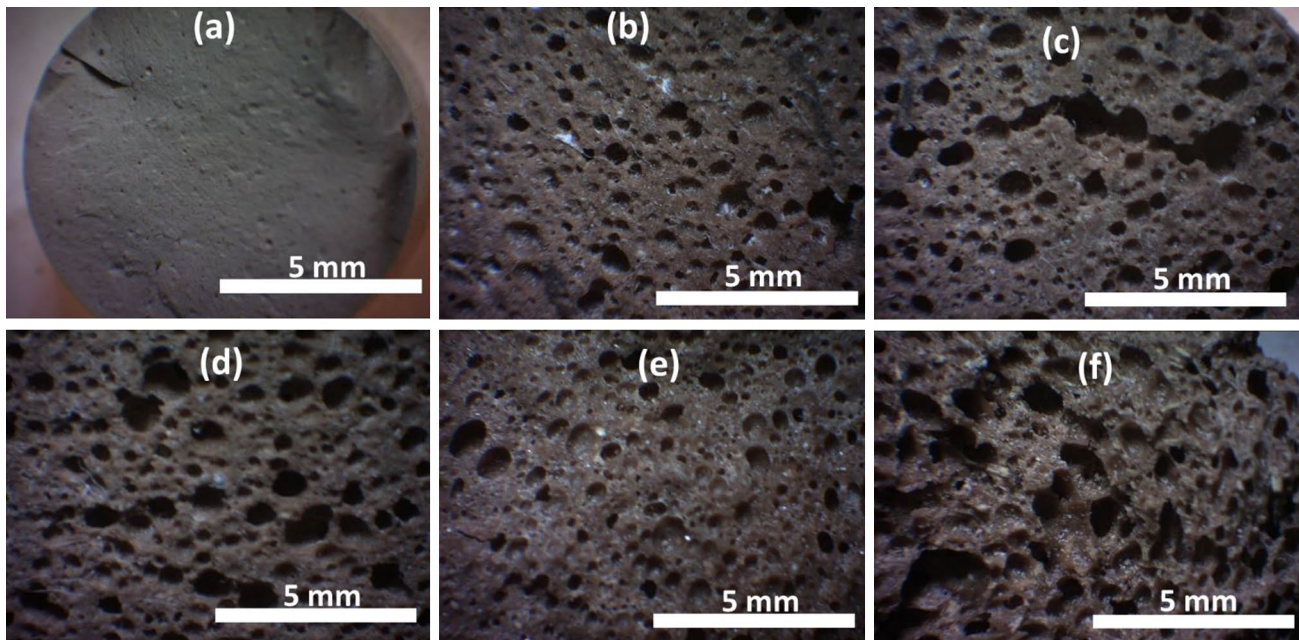


Fig. 7 Optical microscopy photos of **a** MK2-0, **b** MK2-FS, **c** MK2-RHA2-FS, **d** MK2-Sab-FS, **e** MK2-Sa-FS and **f** MK2-S-FS geopolymer samples

3.1.3 Macro and microstructure

3.1.3.1 Geopolymer samples presentation The photos of the resultant geopolymer specimens labelled MK2-0, MK2-FS, MK2-RHA2-FS, MK2-Sab-FS, MK2-Sa-FS and MK2-S-FS are presented in Fig. 6. From this figure, it is observed that reference geopolymer (MK2-0) appeared dense whereas the geopolymer made from metakaolin and additives followed by oven cure at 70 °C exhibited the large pores observable with naked eyes (Fig. 6Aa–f, Ba–f).

The foam structure is generally formed when high reactive material (as silica fume) in alkaline media allows the dehydrogenation reaction causing the appearance of coarse pores linking to increase in porosity within the geopolymer structure [24, 25, 57, 69]. On the other hand the appearance of these pores or voids could be explained by the quick release of water out of geopolymer framework, exhibiting the open cavities along their matrix [27, 32, 70].

3.1.3.2 Macro and microstructure Figure 7 illustrates the photos from optical microscopy (OM) of MK2-0 (Fig. 7a), MK2-FS (Fig. 7b), MK2-RHA-FS (Fig. 7c), MK2-Sa-FS (Fig. 7e), MK2-Sa-FS (Fig. 7e) and MK2-S-FS (Fig. 7f). As described previously, the images showed clearly that the reference sample is dense and the other samples have foam “sponge-like” structure. This foam structure is in agreement with the work of Prud’Homme et al. [22]. The coarse pore in MK2-S-FS sample is more pronounced and appeared as honey comb, with wood fibres. It can also be seen that larger air bubbles having particle size around

3 mm have been formed in sawdust geopolymer foams (Fig. 7f). These open voids are influenced by the incorporation of additive types. For example, in MK2-S-FS sample (Fig. 7f), the depth’ cavities are highly penetrated within the structure while in MK2-S&-FS sample (Fig. 7e), there are smaller opened and randomly distributed in the matrices. The addition of sawdust did not show visual cracks on the surface, sawdust here acted as mechanical reinforcement of geopolymer foams as discussed above.

The microstructures of elaborated geopolymers at lower and higher magnifications are respectively presented in Fig. 8A, B. As observed previously from the optical micrographs (Fig. 7), the reference composition exhibited dense structure (Fig. 7a) while in geopolymers foams (Fig. 7b–f). The sponge like structure as indicated previously is confirmed. There are irregular, inhomogeneous multiscale pores within the geopolymer structure that could reach about 2 mm. Exploring the microstructure at a higher magnification (at 100 μm) (Fig. 8B). One can noticed some structural defects like microcracks and fissures in the reference sample as well as in the foam’s specimens. Nevertheless, these defects are less visible on MK2-S-FS geopolymer thanks to the wood fiber which acted as bridge by reinforcing the mechanical properties as discussed earlier (Paragraph 3.1.2). In comparison to MK2-FS, MK2-RHA-FS, MK2-Sab-FS and MK2-Sa-FS samples, MK2-S-FS formulation containing lignocellulosic material pointed out another pore shape resembling to tubular channels. These channels pores could be benefit for the permeability [71]. In fact, the appearance of microcracks and fissure could be

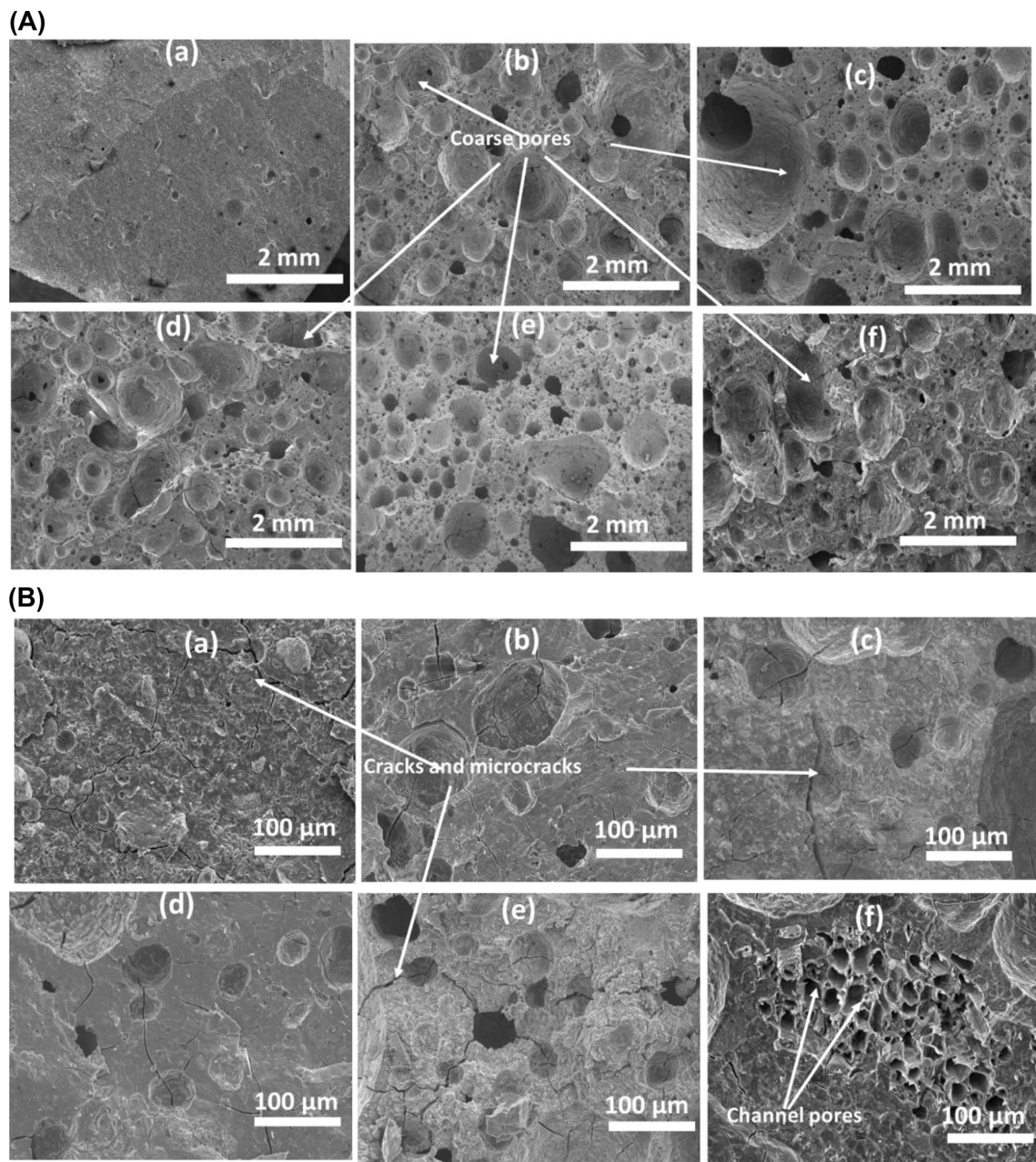


Fig. 8 a Micrographs collected in Secondary electron showing dense structure of MK2-0 sample and sponge like structure of **b** MK2-FS, **c** MK2-RHA2-FS, **d** MK2-Sab-FS, **e** MK2-Sa-FS and **f** MK2-S-FS geopolymer foam samples with coarse pores. **A** Low magnifica-

tion and **B** high magnification showing gel phase embedded inside coarse pores, micro cracks and channels pores from sawdust clearly observed

explained by the fact that at room temperature, the drying is slow and micro-cracks are less important unlike under the oven curing (70 °C). Then the departure of structural water out of the geopolymer network is abrupt resulting in large cracks and fissures. The existence of the channel pore could be related to the reaction that may occur between high reactive amorphous silica from silica fume (Si^0), alkaline solution and hydroxyl group (OH) of cellulose in sawdust thus allowed a little degradation of cellulosic fiber.

3.1.4 Pore connectivity and the distribution of meso and macropores

3.1.4.1 Pore connectivity The data values obtained from MIP analysis in MK2-0, MK2-FS, MK2-RHA-FS, MK2-Sab-FS, MK2-Sa-FS, MK2-S-FS geopolymer samples were outlined in Fig. 9. The plots of cumulative Hg intruded volume as a function of pressure allowing to understand the pore connectivity within the samples is given in Fig. 9A; the plots of

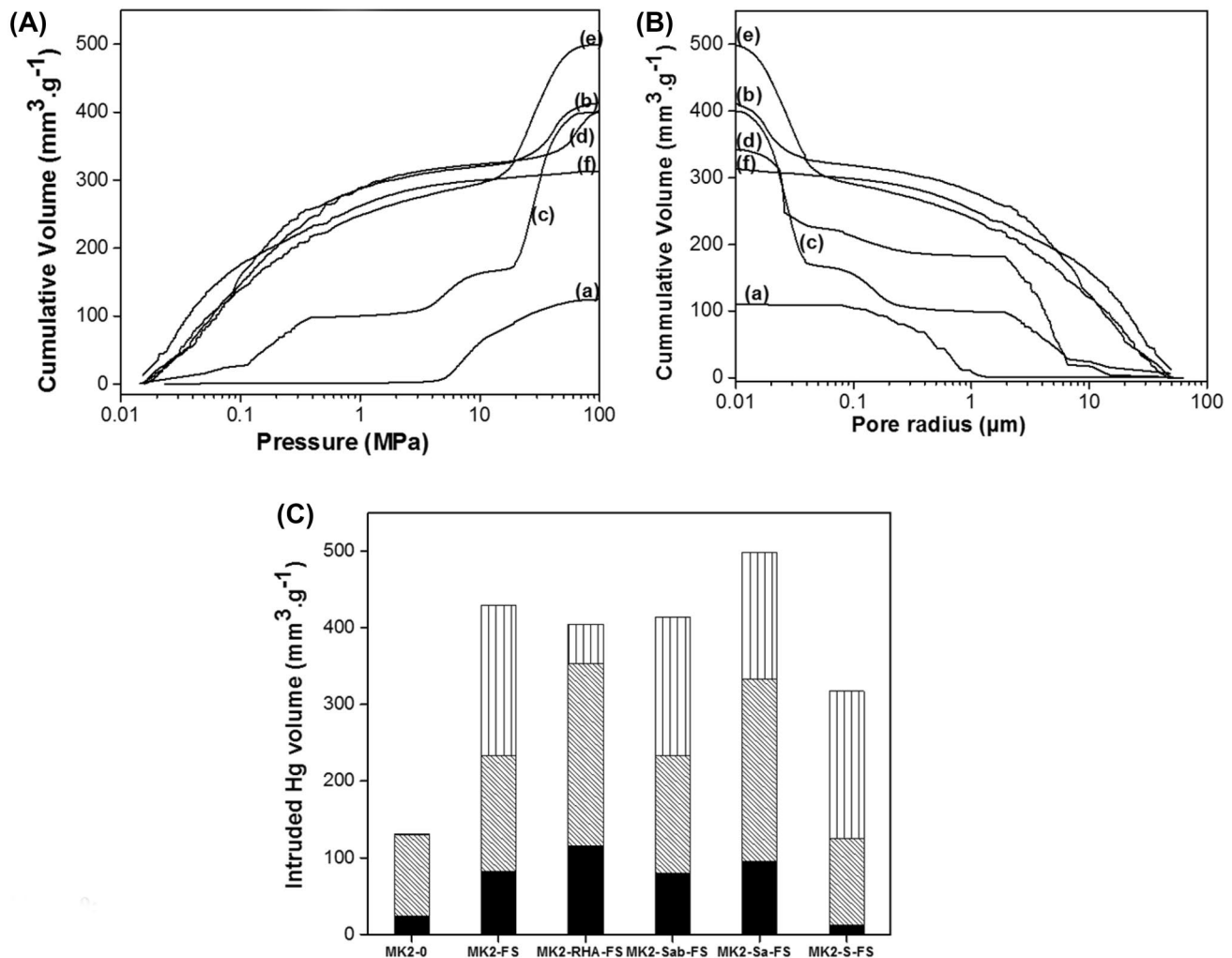


Fig. 9 Plots of cumulative intrusion mercury volume in function of **A** pressure, **B** pore radius of (a) MK2-0, (b) MK2-RHA2-FS, (c) MK2-Sa-FS and (d) MK2-S-FS, MK2-Sa-FS (e) and MK2-S-FS (f) geo-

polymers samples. Distribution of meso ■ ($r < 0.025 \mu\text{m}$), macro ▨ ($0.025 < r < 5 \mu\text{m}$) and coarse ▩ ($r > 5 \mu\text{m}$) pore in geopolymers samples

the cumulative intrusion volume as a function of pore radius in Fig. 9B and finally the pore categories and pore size distribution in Fig. 9C. In fact, the shape of the hysteresis curves qualifies the shape and size range of pores. According to IUPAC, porous media are classified as follow: microporous ($D < 2 \text{ nm}$), meso ($2 \text{ nm} < D < 50 \text{ nm}$) and macropores ($D > 50 \text{ nm}$ where D is the pore diameter). Considering r as pore radius, micron meso, macro and coarse pores respectively corresponded to $r < 0.001 \mu\text{m}$, $0.001 < r < 0.025 \mu\text{m}$, $0.025 < r < 2.5 \mu\text{m}$ and $r > 2.5 \mu\text{m}$ [72–74].

From Fig. 9A, it is emerged that the curve of MK2-0 sample (Fig. 9Aa) did not show many concaves as the curve of geopolymer foams (Fig. 9Ab–f) meaning that the pores in geopolymer foam samples were effectively interconnected.

In Fig. 9B, the reference MK2-0 sample is evidence of bimodal network structure with pore radius centered between 0.05 and $0.1 \mu\text{m}$ while the geopolymer foam are

multimodal with several concaves. This trend is in agreement with the investigation of Malvaut [73]. He explained that the non-homogeneity of the surfaces of high pores connected materials allow the sudden fill up of coarse pores with gas during the MIP analysis. The behaviour of these curves notably the one of MK2-RHA-FS sample is in accordance with the pore size's heterogeneity of the structure.

The total cumulative intrusion volume value ($130.75 \text{ mm}^3 \text{ g}^{-1}$) of MK2-0 was low compared to that of MK2-FS ($426.26 \text{ mm}^3 \text{ g}^{-1}$) sample. The addition of silica fume following by oven curing increased the porosity as observed in Figs. 7, 8 and 9; Table 2 formation of multi-pore scales [1, 24, 57]. When fired sand (Sa) was added, the total cumulative volume increased from 426.26 to $501.66 \text{ mm}^3 \text{ g}^{-1}$ whereas the addition of sawdust (S), rice husk ah (RHA), and unfired sand Sab decreased the total cumulative intrusion volume to 318.63 , 379.20 , and

412.74 mm³ g⁻¹ respectively (Fig. 9A, B). The total porosity from MIP data of MK2-0, MK2-FS, MK2-RHA-FS, MK2-Sab-FS, MK2-Sa-FS and MK2-S-FS geopolymer samples were respectively 19.52, 49.10, 49.14, 47.78, 52.43 and 41.52%. The higher value of open porosity from MIP (diameter ≤ 360 μm) obtained on MK2-Sa-FS sample may be explained by the dissolution of quartz surface in alkaline media (NaOH) through the interaction of quartz and cation (Na⁺) as discussed by Ali et al. [75]. They reported that high alkali cation approach quartz surface and impact hydrolysis of Si–O–Si bond; and due to the basicity of media, OH⁻ break silanol and siloxane surface ligand of quartz lead appears large dimensional cavity of around 20 μm on the surface.

The average pore radius obtained from MIP increases dramatically from 0.106 for MK2-0 to 8.44 μm for MK2-FS corroborating with their total intrusion volume values. But the addition of RHA, Sab, and Sa decreased the average pore radius of geopolymer foams to 0.0275, 0.018, 0.017, 0.027 μm respectively; In contrast, the addition of sawdust increases the average pore radius to 36.92 μm .

3.1.4.2 Meso and macropores distribution The histogram presented in Fig. 9C outlined the frequency distribution of the cumulative Hg intrusion volume as a function of pore size categories in MK2-0, MK2-FS, MK2-RHA-FS, MK2-Sab-FS, MK2-Sa-FS and MK2-S-FS geopolymers samples. The minimum pore radius in the elaborated geopolymers was 0.0037 μm , meaning these samples also contain gel pores which is attributed to the pores with $r \leq 0.015$ [76]. MK2-0 is constituted of meso (18%) and macropores (81%) with the weak presence of coarse pore (0.91%), corroborating with its macro and microstructure (Figs. 6Aa, Ba, 7a, 8Aa, Ba). In contrast, the geopolymer foams were predominated by meso, macro and coarse pores confirming the spongy-like structure of the designed samples (Figs. 6Bb–f, 7b–f, 8Ab–f, Bb–f).

From Fig. 9A, B, one could observe that the addition of silica fume followed by oven curing slightly increases the distribution of mesopores ($0.0125 < r < 0.025$) in overall geopolymer foams except in MK2-S-FS sample. It also increased the percentage of macropores as well as coarse pores (pore with $r > 5$ μm). This confirms the formation of air bubbles through the dehydrogenation reaction [22, 24] as mentioned above.

The details of the meso, macro and coarse pore distribution in foams materials revealed that MK2-Sa-FS and MK2-RHA-FS samples have the highest mesopores (29 and 19% respectively) and macropores (47% and 60% respectively). In contrast, MK2-FS and MK2-S-FS specimens showed more coarse pores percentage (46 and 62% respectively) even though the macropores contributed for 35% in both samples. One can underlined that the better dissolution

of rice hush ash in alkaline solution. However, the reaction onto the surface of silica (quartz sand) described previously may be contributed to the formation of these meso and macropores. These results are in line with the findings of Kamseu et al. [76] who found that the introduction of the foaming agent contributed to increase the number and size of meso and macropores. Although the fact that rice husk ash and sawdust are known as good by-products for the production of lightweight and porous materials [13, 54]. Fine aggregates as quartz sand contributed to the densification of material [77]. Hence, their simultaneous integrating in the matrices with silica fume foam agent [22, 23] in the current work affected the geopolymer network: either by filling the spaces or coarse pores resulting in low pore size distribution, or causing the expansion of the different pore sizes. As partial conclusion, geopolymer with pore size ranging from 0.05 to 1 μm can be prepared with metakaolin without any additives (MK2-0). The elaborated foams undergo three modal pores. The addition of silica fume together with RHA or Sa allowed more meso and macropores foams. While the supplementary addition of sawdust gives high coarse pores materials. The later sample exhibited the interesting mechanical property and will be used for filtration feasibility test.

3.2 Application to the filtration of methylene blue dye

It was obtained from the MIP analysis that the total specific area values of MK2-0, MK2-FS, MK2-RHA2-FS, MK2-Sab-FS, MK2-Sa-FS and MK2-S-FS were 8, 15, 21, 16, 18 and 4 respectively, suggesting that the elaborated sample are able to adsorb pollutant into their surfaces.

The photos of the filtration steps were summarized in Fig. 2. From Fig. 2a, b, it can be seen that water obtained from soaked samples (Fig. 2a) was uncoloured for geopolymer foams with silica additives (Fig. 2b). In contrast, water from MK2-S-FS containing lignocellulosic additive (Fig. 2c) slightly exhibited yellow coloration which disappeared when the filter is washed for several times. The ability of designed filter to remove dye pollutant was evaluated though the filtration of 0.03 g L⁻¹ of Methylene Blue (MB) solution (Fig. 2d). This solution was prepared by the dilution of solution of a commercial solution of Methylene blue (0.5%) with deionized water. The filtration was performed through MK2-S-FS filter sample (Fig. 2e). MK2-Sa-FS and MK2-RHA2 exhibited 3 MPa of compressive strength and could be used as filter but an example of filtration was performed on MK2-S-FS. This formulation was chosen thanks to its high compressive strength (4 MPa) amongst the porous samples elaborated. In fact, filtration process could be carried out at atmospheric pressure or with pressure in order to increase the water flow.

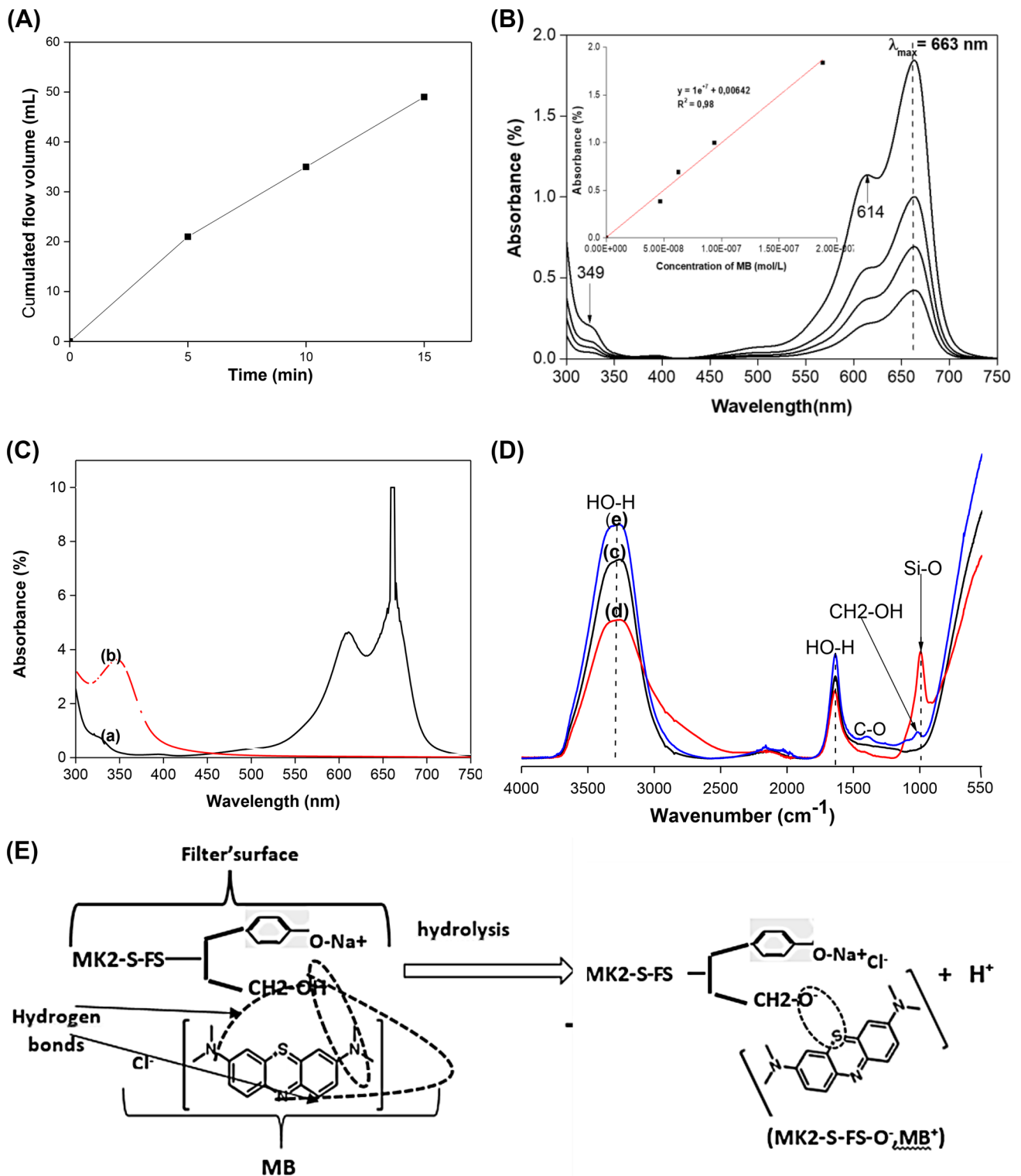


Fig. 10 **A** High flowing volume of sawdust-based geopolymer foam filter and low flowing volume silica-based geopolymer foam filters. **B** UV-Vis spectra of: **A** MB solutions at different concentrations used to plot the calibration curve as a graph of the absorbance at 663 nm as a function of concentration (**b**); initial solution of MB of $0,03 \text{ g L}^{-1}$ (**a**) and its filtrate (**b**) obtained through MK2-S-FS

filter. **C** FT-IR of: deionized water used (**c**, **d**) a solution containing a mixture of water, sawdust, sodium silicate, and sodium hydroxide; and filtrate (**e**) exhibiting the band from organic matter in the filtrate, but the absence of the band of silica and MB band in the filtrate. **E** Proposed reaction mechanism between MK2-S-FS filter surface and MB molecule during the filtration

The explanation that can be given to the choice of the hardest formulation MK2-S-FS (containing sawdust) for filtration is that in one hand, fragile material cannot support high pressure. In another hand, the microstructure of MK2-S-FS displayed channels pores that could be benefit for permeability.

The filtration was performed at atmospheric pressure (1 atm), justifying the great slowly flow of methylene blue (5 mL after 2 days). It's emerged from Fig. 2f that the methylene blue solution inside the filter discoloured with time and the methylene blue particle was attached onto the internal filter's surface. The filtrate was totally blue discoloured, but slightly yellow coloured (Fig. 2g). This yellowed colouration evidently results from organic matter in MK2-S-FS filter as observed earlier (Fig. 2c).

Before the filtration of methylene blue, a permeability test was performed with deionized water. A water flow curve obtained from MK2-S-FS sample (Fig. 10A) revealed that the water flow rate could be about 4 mL min^{-1} . The cumulated flowing volume increases with time confirming the effectiveness of the permeability of the sample [78, 79].

Figure 10B shows the UV-Vis absorption spectra of various MB' concentrations collected in the range of 300–750 nm wavelength. The resulting absorbance values were used to plot the calibration graph which gives the slope (ϵl) used to estimate the filtrate' concentration through the Beer Lambert equation (Eq. 3). This figure displays an intense absorption band at 663 nm and a weak band at 614 nm related respectively to the MB monomer and dimer in aqueous solution [80]. The band at around 300 nm generally occurs at about 293 nm and corresponds to the absorption of aromatic rings. The comparison between the UV-Vis spectrum of the starting solution of MB (0.03 g L^{-1} or $9.53 \times 10^{-5} \text{ mol L}^{-1}$) (Fig. 10Ca) and the spectrum of the filtrate is given in Fig. 10Cb. It is observed that there is plate in the interval of 660 and 668 nm with 10% of absorbance instead of the absorption peak at 663 nm as observed in the previous solutions (Fig. 10Ca). Hence, the saturation occurred during the analysis of the starting solution which still contains many chromophore groups (as observed in the chemical structure of MB) (Fig. 10Bh). This justified by a very intensive blue colour (Fig. 10Bd). The absorption bands of dimer and monomer disappeared on the spectrum of the filtrate (Fig. 10Cb), meaning that there was no chromophore group. In fact, during the filtration process, there are physico-chemical phenomena as electrostatic repulsions which occurred onto the surface of the material [39]. Hence, the filtration of cationic MB⁺ dye in basic medium (pH of 12 from filter used) (Table 2) is benefit for the filtration. The pH of the filtrate was 8.10, confirming that the acid/basic equilibrium reaction was certainly involved between the two species.

In order to evaluate the efficiency of MB removal with designed filter the concentration of MB in the filtrate was calculated using the molar absorptivity ϵ of $7 \text{ L mol}^{-1} \text{ cm}^{-1}$ obtained from the calibration curve given in Fig. 10B and Eq. 3. From Fig. 10B, the absorbance of the filtrate was 0.03% which corresponds to a concentration of $1.5 \times 10^{-9} \text{ mol L}^{-1}$ or $4.79 \times 10^{-7} \text{ g L}^{-1}$ of MB. So, the percentage of removal estimated from Eq. 4 was 99.9%. This result confirms the effectiveness of the elaborated filter for methylene blue filtration. However, the absorption band at $\sim 349 \text{ nm}$ in UV region corresponding to the absorption of the aromatic nucleus increased on the spectrum of the filtrate (Fig. 10Cb). This indicates the presence of aromatic ring, certainly from wood fiber, similar to the color observed on the photo of water after soaking the filter (Fig. 2c). The filter was directly used after soaking for 24 h and was not washed several times, this justifies both yellowish coloration in Fig. 2c, g.

The confirmation of the MB removal was also confirmed by FT-IR analysis of some solutions between 400 and 4000 cm^{-1} (Fig. 10C). Methylene blue molecule (Fig. 2h) contains several chemical bonds that can be detected by FT-IR spectroscopy. These chemical bonds [80] include: C–S ($700\text{--}600 \text{ cm}^{-1}$), C=C aromatic ($730\text{--}665 \text{ cm}^{-1}$), aromatic C=C ($1600\text{--}1450 \text{ cm}^{-1}$), CN 1st amino ($772\text{--}665 \text{ cm}^{-1}$), CN amino 2nd ($1220\text{--}1020 \text{ cm}^{-1}$), aromatic CH ($860\text{--}800 \text{ cm}^{-1}$), aromatic CH ($1175\text{--}1125 \text{ cm}^{-1}$), CH (aliphatic CH₃) ($1398\text{--}1385 \text{ cm}^{-1}$), CH₂ aliphatic CH₂ ($2975\text{--}2950 \text{ cm}^{-1}$), and NH₂ amine ($3500\text{--}3100 \text{ cm}^{-1}$). But, almost all of these bands were not practically found on the spectrum of the filtrate. The FT-IR spectra of the deionized water (Fig. 10Dc), filtrate (Fig. 10De) a solution from a mixture of sodium silicate, NaOH, sawdust and distilled water (Fig. 10Dd) were studied. The last was interest to observe the band from silicate and organic material therefore to confront their result to the FT-IR spectrum of the filtrate. The FT-IR spectra of methylene blue [80] and sawdust [42, 81] were referred to the literature data. There were found on the three spectra (Fig. 10Dc–e) evidently the stretching of the broad bands of water at 3280 and 1630 cm^{-1} . The spectrum of the solution containing sodium silicate (Fig. 10Dd) pointed out the stretching band of Si–O from silica in the medium. One can noticed the presence of two weak bands on the FT-IR spectra of the filtrate at $\sim 1388 \text{ cm}^{-1}$ and $\sim 1002 \text{ cm}^{-1}$. The first band could be attributed to the stretching of C–O bond from carbonate. The second is related either to the vibration of CH₂OH group from sawdust, or from another Si–O bond, if so, it will mean that the siliceous species have leached and pass through the solution. However, this hypothesis will be confirmed by further analysis as X-R Spectro fluorescence. Moreover, it is likely the columbic attraction and hydrogen bond are occurred trough the alkali hydrolysis

of the surface of MK2-S-FS filter structured by OH from cellulosic sawdust and the molecule of methylene blue which is acid/base dye. Interestingly, the good removal increase of the MB was favoured the high pH operating range as reported by some researchers [35, 80, 82] the adsorption with the increase in high pH media as concluded. The mechanism of reaction the electronic attraction and/or hydrolysis onto the surface's filter could be proposed on Fig. 10E showed the possibility of the formation of complex in accordance with the work of Paulino et al. [37].

4 Conclusion

The effect of silica and lignocellulosic additives on the microstructure and pore size distribution of metakaolin/silica fume-based geopolymer foams filters consolidated at 70 °C was achieved in this work. It was found that:

- A replacement of metakaolin powder by 21% of silica fume (FS) used as foaming agent was suitable to prepare sponge material, but this formulation exhibited very low mechanical property. Then, 25 wt% of FS and 12.5wt % of additives (RHA, Sab, Sa, or S) were simultaneously added to aluminosilicates (MK2) therefore to vary the pore network distribution. This increases the theoretical Si/Al molar ratio respectively from 3.72 to 4.28, explaining the low compressive strength due to a low polycondensation.
 - Microstructure of geopolymer foams, foams displayed heterogeneously multipore scales randomly distributed, consisted of gel, meso, macro and air void pores (coarse pores) with remarkably appearance of tubular channels pores in the microstructure of sawdust-based foams. However, the oven curing allowed microcracks within the system.
 - Additives used here significantly affected the pore size distribution evaluated as vol%. For instance, MK2-RHA-FS with average pore radius of 0.27 µm was the specimen containing the higher 29 vol% in meso pores range ($0.00125 < r < 0.025$ µm); MK2-Sa-FS sample with an average pore radius of 0.27 µm exhibited 47 vol% of TCIV (Total Cumulative Intrusion Volume) in macropores range. In geopolymer foams MK2-S-FS and MK2-FS with average pore radius of 369.26 and 84.42 µm respectively, it was pointed out that 45 and 60 vol% contributed to air voids pores or coarse pores ($r > 5$ µm). Hence, the low average pore radius of 0.18–1 µm were from MK2-RHA-FS and MK2-Sa-FS samples and high pore radius (84–369 µm) obtained from MK2-FS, MK2-Sab-FS and MK2-S-FS in agreement with their macro and microstructure.
- The designed materials geopolymer foams were highly porous, and permeable. Thus, prominent candidate for macro filtration. However, an attention needs to be paid in the oven curing to avoid or reduce various cracks formation. An example of methylene blue filtration revealed that MK2-S-FS filter, the hardest specimen was suitable to remove methylene blue dye in aqueous solution with 99.9% dye removal thanks to the ionic exchange and probably complexation reaction occurring onto the surface of filter. In the further works, we will study the performance of filter when under a pressure gradient. The evaluation of bacterial removal is also projected in future works.

Acknowledgements The authors thank the AUF-BACGL (Agence Universitaire de la Francophonie, Bureau Afrique Centrale et Grands Lacs) for their financial support (Grant S0020ADM10604L, 2017–2019).

Compliance with ethical standards

Conflict of interest The authors declare that they have no conflict of interest.

References

1. Davidovits J (1991) Geopolymers—*inorganic polymeric new materials*. *J Therm Anal* 37:1633–1656. <https://doi.org/10.1007/BF01912193>
2. Davidovits J (1994) Properties of geopolymer cements. In: *First international conference on alkaline cements and concretes science research institute binding mater*, KIEV, State Technical University, Ukraine, pp 131–149
3. Duxson P, Fernández-Jiménez A, Provis JL, Lukey GC, Palomo A, Van Deventer JSJ (2007) Geopolymer technology: the current state of the art. *J Mater Sci*. <https://doi.org/10.1007/s10853-006-0637-z>
4. Davidovits J (2015) *Geopolymer chemistry and applications*, 4th edn. Institut Géopolymère, Saint Quentin
5. Cheng TW, Lee ML, Ko MS, Ueng TH, Yang SF (2012) The heavy metal adsorption characteristics on metakaolin-based geopolymer. *Appl Clay Sci* 56:90–96. <https://doi.org/10.1016/j.clay.2011.11.027>
6. Rambure KK (2013) *Vers de nouvelles matrices minérales pour l'immobilisation et la valorisation des déchets ultimes de l'incinération des déchets ménagers*, Thèse Dr. Univ. Paris-Est, Fr, 357p
7. López FJ, Sugita S, Tagaya M, Kobayashi T (2014) Metakaolin-based geopolymers for targeted adsorbents to heavy metal ion separation. *J Mater Sci Chem Eng* 2:16–27. <https://doi.org/10.4236/msce.2014.27002>
8. Mallicoat S, Sarin P, Kriven WM (2008) Novel, alkali-bonded, ceramic filtration membranes. In: *Developments in advanced ceramics and composites: a collection of papers presented at the 29th international conference on advanced ceramics and composites*, January 23–28, 2005, Cocoa Beach, Florida. 26 (N8), pp 37–44. <https://doi.org/10.1002/9780470291283.ch5>

9. Jing L, Yan H, Yuan Y, Jing-lin H, Xue-min C (2014) The preparation and characterization of geopolymer based inorganic membranes. *Key Eng Mater* 602–603:80–83. <https://doi.org/10.4028/www.scientific.net/KEM.602-603.80>
10. Xu M, He Y, Wang C, He X, He X, Liu J, Cui X (2015) Applied clay science preparation and characterization of a self-supporting inorganic membrane based on metakaolin-based geopolymers. *Appl Clay Sci* 115:4–9. <https://doi.org/10.1016/j.clay.2015.03.019>
11. Ge Y, Yuan Y, Wang K, He Y, Cui X (2015) Preparation of geopolymer-based inorganic membrane for removing Ni²⁺ from wastewater. *J Hazard Mater* 299:711–718. <https://doi.org/10.1016/j.jhazmat.2015.08.006>
12. Lin K-L, Lan J-Y (2013) Water retention characteristics of porous ceramics produced from waste diatomite and coal fly ash. *J Clean Energy Technol* 1:211–215. <https://doi.org/10.7763/JOCET.2013.V1.48>
13. Fongang RTT, Pemndje J, Lemougna PN, Melo UC, Nanseu CP, Nait-Ali B, Kamseu E, Leonelli C (2015) Cleaner production of the lightweight insulating composites: microstructure, pore network and thermal conductivity. *Energy Build* 107:113–122. <https://doi.org/10.1016/j.enbuild.2015.08.009>
14. Ngouloure ZNM, Nait-ali B, Zekeng S, Kamseu E, Melo UC, Smith D, Leonelli C (2015) Recycled natural wastes in metakaolin based porous geopolymers for insulating applications. *J Build Eng* 3:58–69. <https://doi.org/10.1016/j.jobe.2015.06.006>
15. Kamseu E, Boccaccini DN, Sola A, Rizzuti A, Leonelli C, Melo UC, Billong N (2008) Sintering behaviour, microstructure and mechanical properties of low quartz content vitrified ceramics using volcanic ash. *Adv Appl Ceram* 107:19–27. <https://doi.org/10.1179/174367607X227981>
16. Kamseu E, Bignozzi MC, Melo UC, Leonelli C, Sglavo VM (2013) Design of inorganic polymer cements: effects of matrix strengthening on microstructure. *Constr Build Mater* 38:1135–1145. <https://doi.org/10.1016/j.conbuildmat.2012.09.033>
17. Tippayasam C, Boonanonwong P, Calvez J, Thavorniti P, Chindaprasirt P, Chaysuwan D (2016) Effect of porosity and pore size on microstructures and mechanical properties of metakaolin blended with Ca(OH)₂ and PLA as porous geopolymers. *Key Eng Mater* 690:276–281. <https://doi.org/10.4028/www.scientific.net/KEM.690.276>
18. López FJ, Sugita S, Tagaya M, Kobayashi T (2014) Geopolymers using rice husk silica and metakaolin derivatives; preparation and their characteristics. *J Mater Sci Chem Eng* 2:35–43. <https://doi.org/10.4236/msce.2014.25006>
19. Evans EL, Gavrilovich TC, Mihai E, Isbasescu RC, Evans Gavrilovich E, Mihai RC, Isbasescu I, Easyg EL, Evans TC, Gavrilovich E, Mihai RC, Isbasescu I (2015) Patent application publication (10) Pub. No: US 2006/0222585 A1 Figure 1, 002:354. <https://doi.org/10.1037/t24245-000>
20. Yan L, Kasal B, Huang L (2016) A review of recent research on the use of cellulosic fibres, their fibre fabric reinforced cementitious, geo-polymer and polymer composites in civil engineering. *Compos Part B Eng* 92:94–132. <https://doi.org/10.1016/j.compositesb.2016.02.002>
21. Rasouli HR, Golestani-Fard F, Mirhabibi AR, Nasab GM, MacKenzie KJD, Shahraki MH (2015) Fabrication and properties of microporous metakaolin-based geopolymer bodies with polylactic acid (PLA) fibers as pore generators. *Ceram Int* 41:7872–7880. <https://doi.org/10.1016/j.ceramint.2015.02.125>
22. Prud E, Michaud P, Joussein E, Peyratout C, Smith A, Arrii-clacens S, Clacens JM, Rossignol S (2010) Silica fume as porogen agent in geo-materials at low temperature. *J Eur Ceram Soc* 30:1641–1648. <https://doi.org/10.1016/j.jeurceramsoc.2010.01.014>
23. Khater HM (2013) Effect of silica fume on the characterization of the geopolymer materials. *Int J Adv Struct Eng* 5:1–10. <https://doi.org/10.1186/2008-6695-5-12>
24. Papa E, Medri V, Kpogbemabou D, Morinière V, Laumonier J, Vaccari A, Rossignol S (2016) Porosity and insulating properties of silica-fume based foams. *Energy Build*. <https://doi.org/10.1016/j.enbuild.2016.09.031>
25. Luna-GalianoLeiva Y, Leiva C, Arenas C, Ferdàndez-Pereira C (2018) Fly ash based geopolymeric foams using silica fume as pore generation agent Physical, mechanical and acoustic properties. *J Non-Cryst Solids*. <https://doi.org/10.1016/j.jnoncrysol.2018.07.069>
26. Tognonvi MT, Soro J, Rossignol S (2012) Durability of tubular geopolymer reinforced with silica sand. *New J Glass Ceram* 2012:85–90
27. Sindhunata JSJ, Van Deventer J, Lukey GC, Xu H (2006) Effect of curing temperature and silicate concentration on fly-ash-based geopolymerization. *Ind Eng Chem Res* 45:3559–3568
28. Rovnanik P, Al SO (2010) Effect of curing temperature on the development of hard structure of metakaolin-based geopolymer. *Constr Build Mater* 24:1176–1183. <https://doi.org/10.1016/j.conbuildmat.2009.12.023>
29. PrudHomme E, Michaud P, Joussein E, Clacens JM, Rossignol S (2011) Role of alkaline cations and water content on geo-material foams: monitoring during formation. *J Non-Cryst Solids* 357:1270–1278. <https://doi.org/10.1016/j.jnoncrysol.2010.12.030>
30. Muñiz-Villarreal MS, Manzano-Ramírez A, Sampieri-Bulbarela S, Gasca-Tirado JR, Reyes-Araiza JL, Rubio-Ávalos JC, Pérez-Bueno JJ, Apatiga LM, Zaldivar-Cadena A, Amigó-Borrás V (2011) The effect of temperature on the geopolymerization process of a metakaolin-based geopolymer. *Mater Lett* 65:995–998. <https://doi.org/10.1016/j.matlet.2010.12.049>
31. Feng J, Zhang R, Gong L, Li Y, Cao W, Cheng X (2015) Development of porous fly ash-based geopolymer with low thermal conductivity. *Mater Des* 65:529–533. <https://doi.org/10.1016/j.matdes.2014.09.024>
32. Siyal AA, Azizli KA, Man Z, Ullah H (2016) Effects of parameters on the setting time of fly ash based geopolymers using Taguchi method. *Procedia Eng* 148:302–307. <https://doi.org/10.1016/j.proeng.2016.06.624>
33. Nasvi MCM, Ranjith PG, Sanjayan J, Bui H (2014) Effect of temperature on permeability of geopolymer: a primary well sealant for carbon capture and storage wells. *Fuel* 117:354–363. <https://doi.org/10.1016/j.fuel.2013.09.007>
34. Childs EC, Collis-George GN (1950) The permeability of porous materials. *Proc R Soc Lond Ser A* 201:392–405
35. Al-Ghouti MA, Khraisheh MAM, Allen SJ, Ahmad MN (2003) The removal of dyes from textile wastewater: a study of the physical characteristics and adsorption mechanisms of diatomaceous earth. *J Environ Manag* 69:229–238. <https://doi.org/10.1016/j.jenvman.2003.09.005>
36. Hameed BH, Din ATM, Ahmad AL (2007) Adsorption of methylene blue onto bamboo-based activated carbon: kinetics and equilibrium studies. *J Hazard Mater* 141(141):819–825. <https://doi.org/10.1016/j.jhazmat.2006.07.049>
37. Paulino AT, Guilherme MR, Reis AV, Campese GM, Muniz EC, Nozaki J (2006) Removal of methylene blue dye from an aqueous media using superabsorbent hydrogel supported on modified polysaccharide. *J Colloid Interface Sci* 301:55–62. <https://doi.org/10.1016/j.jcis.2006.04.036>
38. Bamouni F (2016) Élimination de Bleu de Méthylène en solution aqueuse par un matériau hybride à base d'oxydes de Manganèse et de Charbon actif, Mémoire Master, Inst. Int. d'Ingénierie, Ouagadougou, Bukina-Faso, 62p
39. Epinasse B (2003) Approche théorique et expérimentale de la filtration tangentielle de colloïdes: flux et colmatage, Thèse Dr. Univ. Toulouse III, Toulouse, France, 213p

40. Calabro V, Pantano G, Kang M, Molinari R, Drioli E (1990) Experimental study on integrated membrane processes in the treatment of solutions simulating textile effluents. *Energy Exergy Anal Desalinat* 78:257–277
41. Bai C, Colombo P (2017) High-porosity geopolymer membrane supports by peroxide route with the addition of egg white as surfactant. *Ceram Int* 43:2267–2273. <https://doi.org/10.1016/j.ceramint.2016.10.205>
42. Youmoue M, Fongang RTT, Gonidanga SB, Likiby B, Gharzouni A, Kamseu E, Tonle IK, Rossignol S Metakaolin-based geopolymers materials: effect of silica and lignocellulosic additives on the kinetic of geopolymerization through ATR-FTIR spectrometry, the mechanical properties and microstructure. *Ceram Mod Technol (CMT-D-19-00012R1)*, accepted for publication
43. Fernandes HR, Tulyaganov DU, Ferreira JMF (2009) Preparation and characterization of foams from sheet glass and fly ash using carbonates as foaming agents. *Ceram Int* 35:229–235. <https://doi.org/10.1016/j.ceramint.2007.10.019>
44. Zhang Y, Sun W, Li Z (2008) Infrared spectroscopy study of structural nature of geopolymeric products. *J Wuhan Univ Technol Mater Sci Ed* 23:522–527. <https://doi.org/10.1007/s11595-007-4522-7>
45. Atef A, Joussein E, Gasgnier G, Rossignol S (2012) Role of the silica source on the geopolymerization rate. *J Non-Cryst Solids* 358:2886–2893. <https://doi.org/10.1016/j.jnoncrysol.2012.07.015>
46. Šćiban M, Klačnjak M, Škrbic M (2006) Modified softwood sawdust as adsorbent of heavy metal ions from water. *J Hazard Mater B* 136:266–271. <https://doi.org/10.1016/j.jhazmat.2005.12.009>
47. Djilali Y, Elandaloussi EH (2012) Alkaline treatment of timber sawdust: a straightforward route toward effective low-cost adsorbent for the enhanced removal of basic dyes from aqueous solutions. *J Saudi Chem Soc.* <https://doi.org/10.1016/j.jscs.2012.10.013>
48. Kenne Dedzo G, Péguy Nanseu-Njiki C, Ngameni E (2012) Amperometric sensors based on sawdust film modified electrodes: application to the electroanalysis of paraquat. *Talanta* 99:478–486. <https://doi.org/10.1016/j.talanta.2012.06.013>
49. Nagy B, Mánzatu C, Andrada M, Indolean C, Silaghi-Dumitrescu L, Majdik C (2014) Journal of wood chemistry and effect of alkaline and oxidative treatment on sawdust capacity to remove Cd (II) from aqueous solutions: FTIR and AFM study. *J Wood Chem Technol* 34:37–41. <https://doi.org/10.1080/02773813.2013.875040>
50. Kim B, Gulati I, Park J, Shin J-S (2012) Pretreatment of cellulosic waste sawdust into reducing sugars using mercerization and etherification. *BioResources* 7:5152–5166
51. Lin M, Pei Z, Lei S (2017) Mineralogy and processing of hydrothermal vein quartz from Hengche, Hubei Province (China). *Minerals* 7:1–16. <https://doi.org/10.3390/min7090161>
52. Maulana AI, Wardani NK, Syamsidar D (2017) Development of hybrid composite rice husk ash (RHA)—geopolymer for bricks bearing buildings. *MATEC Web Conf* 97(01009):1–8. <https://doi.org/10.1051/mateconf/20179701009>
53. Kaur K, Singh J, Kaur M (2018) Compressive strength of rice husk ash based geopolymer: the effect of alkaline activator. *Constr Build Mater J* 169:188–192. <https://doi.org/10.1016/j.conbuildmat.2018.02.200>
54. Detphan S, Chindaprasirt P (2009) Preparation of fly ash and rice husk ash geopolymer. *Int J Miner Metall Mater* 16:720–726. [https://doi.org/10.1016/S1674-4799\(10\)60019-2](https://doi.org/10.1016/S1674-4799(10)60019-2)
55. Kaze RC, Myllylam L, Moungam B, Cannio M, Rosa R, Kamseu E, Melo UC, Leonelli C (2018) Microstructure and engineering properties of Fe₂O₃(FeO)-Al₂O₃-SiO₂ based geopolymer composites. *J Clean Prod.* <https://doi.org/10.1016/j.jclepro.2018.07.171>
56. Rees CA, Provis JL, Lukey GC, Van Deventer JSJ (2007) In situ ATR-FTIR study of the early stages of fly ash geopolymer gel formation. *Langmuir* 23:9076–9082
57. Prudhomme E (2011) Rôles du cation alcalin et des renforts minéraux et végétaux sur les mécanismes de formation de géopolymères poreux ou denses, 264p
58. Bignozzi Chiara M, Manzi S, Natali Elia M, Rickard WDA, Van Riesen A (2014) Room temperature alkali activation of fly ash: the effect of Na²O/SiO₂ ratio. *Constr Build Mater* 69:262–270. <https://doi.org/10.1016/j.conbuildmat.2014.07.062>
59. Rocha S, Dias DP, César F, França C, Rangel R, Guerra DS, Rodrigues L, Marques DO (2018) Metakaolin-based geopolymer mortars with different alkaline activators. *Constr Build Mater* 178:453–461. <https://doi.org/10.1016/j.conbuildmat.2018.05.172>
60. Tchakouté HK, Rüscher CH, Kong S, Kamseu E, Leonelli C (2017) Thermal behavior of metakaolin-based geopolymer cements using sodium waterglass from rice husk ash and waste glass as alternative activators. *Waste Biomass Valoriz* 8:573–584. <https://doi.org/10.1007/s12649-016-9653-7>
61. Ulloa CA, Gordon AL, García XA (2009) Thermogravimetric study of interactions in the pyrolysis of blends of coal with radiata pine sawdust. *Fuel Process Technol* 90:583–590. <https://doi.org/10.1016/j.fuproc.2008.12.015>
62. Gao N, Li A, Quan C, Du L, Duan Y (2013) TG-FTIR and Py-GC/MS analysis on pyrolysis and combustion of pine sawdust. *J Anal Appl Pyrolysis* 100:26–32. <https://doi.org/10.1016/j.jaap.2012.11.009>
63. Chen G, Leung DY (2014) Experimental investigation of biomass waste (rice straw, cotton stalk, and pine sawdust). *Pyrolysis Charact Energy Resour* 25:37–41. <https://doi.org/10.1080/009083190142361>
64. Istuque DB, Reig L, Moraes JCB, Akasaki JL, Borrachero MV, Soriano L, Payá J, Malmonge JA, Tashima MM (2016) Behaviour of metakaolin-based geopolymers incorporating sewage sludge ash (SSA). *Mat Lett* 180:192–195
65. Duan P, Yan C, Zhou W, Luo W (2016) Fresh properties, mechanical strength and microstructure of fly ash geopolymer paste reinforced with sawdust. *Constr Build Mater* 111:600–610
66. Ramos M, Valdés A, Garrigós MC (2016) Multifunctional applications of nanocellulose-based nanocomposites. Elsevier Inc. <https://doi.org/10.1016/b978-0-323-44248-0.00006-7>
67. Fortunati E, Kenny M, Torre L (2019) Lignocellulosic materials as reinforcements in sustainable packaging systems: processing, properties, and applications. *Biomass Biopolym Mater Bioenergy* 5:87–102. <https://doi.org/10.1016/B978-0-08-102426-3.00005-9>
68. Bai C, Colombo P (2018) Processing, properties and applications of highly porous geopolymers: a review. *Ceram Int* 44(14):16103–16118. <https://doi.org/10.1016/j.ceramint.2018.05.219>
69. Prudhomme E, Michaud P, Joussein E, Smith A, Peyratout C, Sobrados I, Sanz J, Rossignol S (2012) Geomaterial foams: role assignment of raw materials in the network formation. *J Sol-Gel Sci Technol* 61:436–448. <https://doi.org/10.1007/s10971-011-2644-z>
70. Zhang Z, Provis JL, Reid A, Wang H (2014) Geopolymer foam concrete: an emerging material for sustainable construction. *Constr Build Mater* 56:113–127. <https://doi.org/10.1016/j.conbuildmat.2014.01.081>
71. Simonis JJ, Basson AK (2012) Manufacturing a low-cost ceramic water filter and filter system for the elimination of common pathogenic bacteria. *Phys Chem Earth* 50–52:269–276. <https://doi.org/10.1016/j.pce.2012.05.001>
72. Zdravkov BD, Čermák JJ, Šefara M, Janků J (2007) Pore classification in the characterization of porous materials: a perspective.

- Cent Eur J Chem 5(2):385–395. <https://doi.org/10.2478/s11532-007-0017-9>
73. Malvault G (2013) Détermination expérimentale de la distribution de taille de pores d'un milieu poreux par l'injection d'un fluide à seuil ou analyse harmonique, École Nationale Supérieure d'Arts et Métiers, Paris, France, 178p
74. Rao SM (2017) Mercury intrusion porosimetry studies with geopolymers. *Indian Geotech J* 47:495–502. <https://doi.org/10.1007/s40098-017-0245-7>
75. Ali AM, Padmanabhan E, Baioumy H (2017) Characterization of alkali-induced quartz dissolution rates and morphologies. *Arab J Sci Eng* 42:2501–2513. <https://doi.org/10.1007/s13369-017-2483-5>
76. Kamseu E, Nait-Ali B, Bignozzi MC, Leonelli C, Rossignol S, Smith DS (2012) Bulk composition and microstructure dependence of effective thermal conductivity of porous inorganic polymer cements. *J Eur Ceram Soc* 32:1593–1603. <https://doi.org/10.1016/j.jeurceramsoc.2011.12.030>
77. Kamseu E, Ponzoni C, Tippayasam C, Taurino R, Chaysuwan D, Chiara M, Barbieri L, Leonelli C (2015) Influence of fine aggregates on the microstructure, porosity and chemico-mechanical stability of inorganic polymer concretes. *Constr Build Mater* 96:473–483. <https://doi.org/10.1016/j.conbuildmat.2015.08.090>
78. Belibi PB, Nguemtchouin MMG, Rivallin M, Nsami JN, Sieliechi J (2015) Micro filtration ceramic membranes from local Cameroonian clay applicable to water treatment. *Ceram Int* 41:2752–2759. <https://doi.org/10.1016/j.ceramint.2014.10.090>
79. Youmoue M, Fongang RTT, Sofack JC, Kamseu E, Melo UC, Tonle IK, Leonelli C, Rossignol S (2017) Design of ceramic filters using Clay/Sawdust composites: effect of pore network on the hydraulic permeability. *Ceram Int* 43:4496–4507. <https://doi.org/10.1016/j.ceramint.2016.12.101>
80. Yan Y, Zhang M, Gong K, Su L, Guo Z, Mao L (2005) Adsorption of methylene blue dye onto carbon nanotubes: a route to an electrochemically functional nanostructure and its layer-by-layer assembled nanocomposite. *Chem Mater* 17:3457–3463
81. Benyoucef S, Harrache D (2015) Caractérisation de la microstructure de sciure de bois de pin sylvestre "*Pinus sylvestris*". *J Mater Environ Sci* 6:765–772
82. Tonle IK, Ngameni E, Walcarius A (2008) Sorption of methylene blue on an organoclay bearing thiol groups and application to electrochemical sensing of the dye. *Talanta* 74:489–497. <https://doi.org/10.1016/j.talanta.2007.06.006>

Publisher's Note Springer Nature remains neutral with regard to jurisdictional claims in published maps and institutional affiliations.